



US 20240051018A1

(19) **United States**

(12) **Patent Application Publication**
EBISU

(10) **Pub. No.: US 2024/0051018 A1**

(43) **Pub. Date: Feb. 15, 2024**

(54) **UNIDIRECTIONAL SOLIDIFICATION DEVICE, UNIDIRECTIONAL SOLIDIFICATION METHOD, UNIDIRECTIONALLY SOLIDIFIED CASTING, AND UNIDIRECTIONALLY SOLIDIFIED INGOT**

(52) **U.S. Cl.**
CPC **B22D 27/045** (2013.01); **B22D 27/02** (2013.01); **B22D 27/003** (2013.01)

(57) **ABSTRACT**

(71) Applicant: **EBIS CORPORATION**, Sagamihara (JP)

(72) Inventor: **Yoshio EBISU**, Sagamihara (JP)

(73) Assignee: **EBIS CORPORATION**, Sagamihara (JP)

(21) Appl. No.: **18/277,800**

(22) PCT Filed: **Feb. 3, 2022**

(86) PCT No.: **PCT/JP2022/004291**

§ 371 (c)(1),

(2) Date: **Aug. 18, 2023**

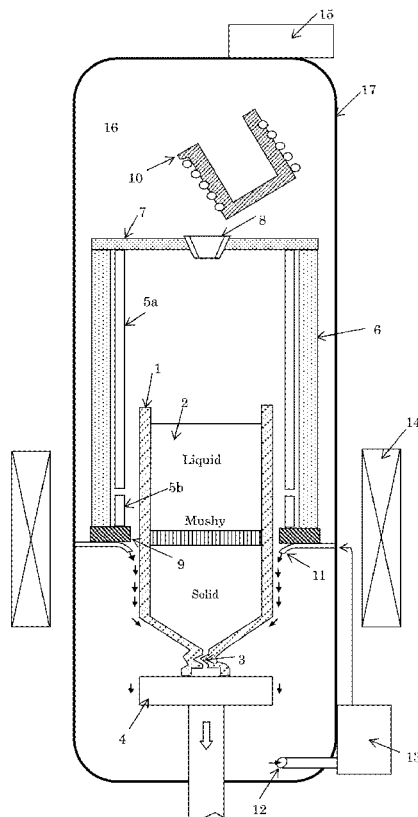
(30) **Foreign Application Priority Data**

Feb. 24, 2021 (JP) 2021-067999

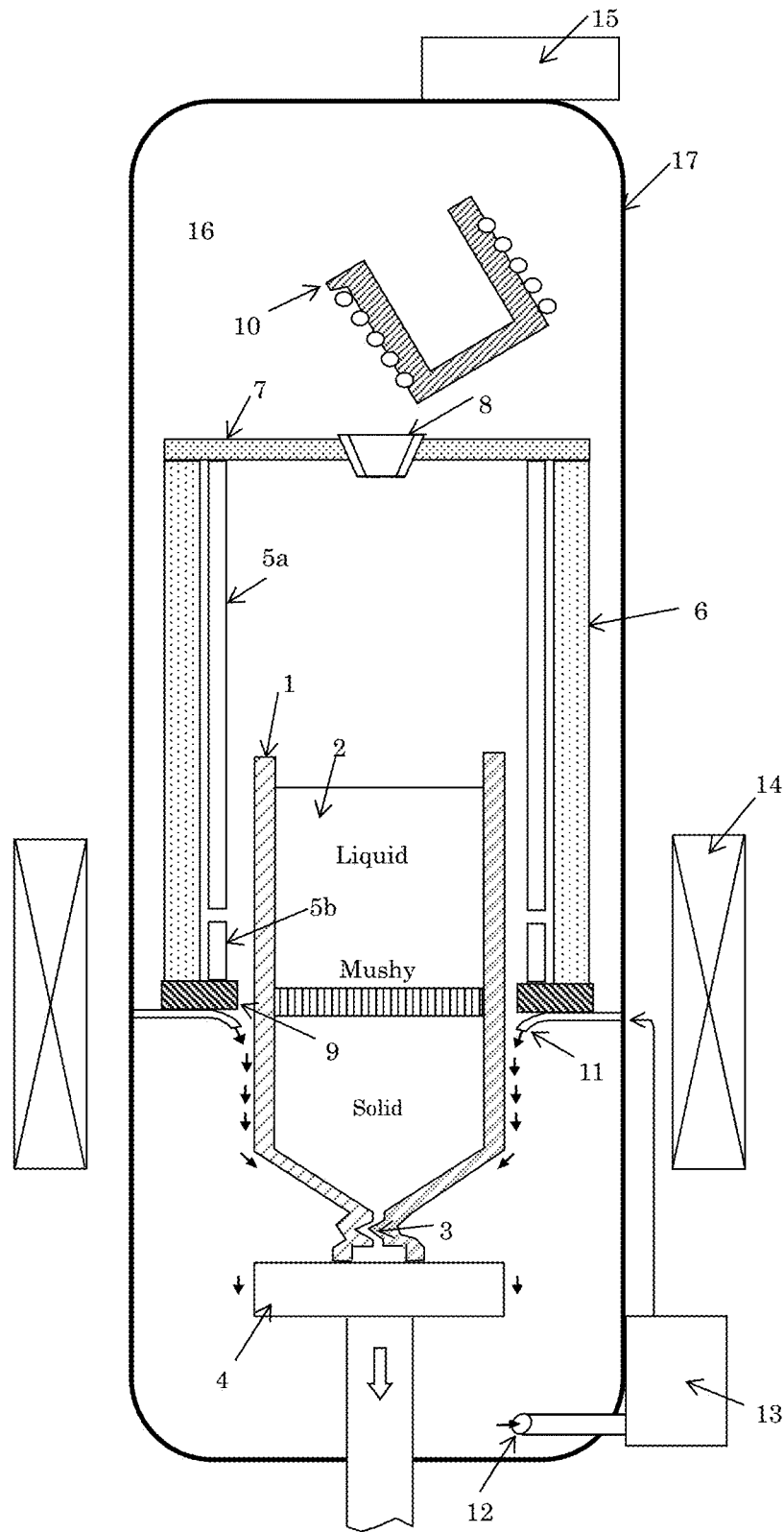
Publication Classification

(51) **Int. Cl.**
B22D 27/04 (2006.01)
B22D 27/02 (2006.01)
B22D 27/00 (2006.01)

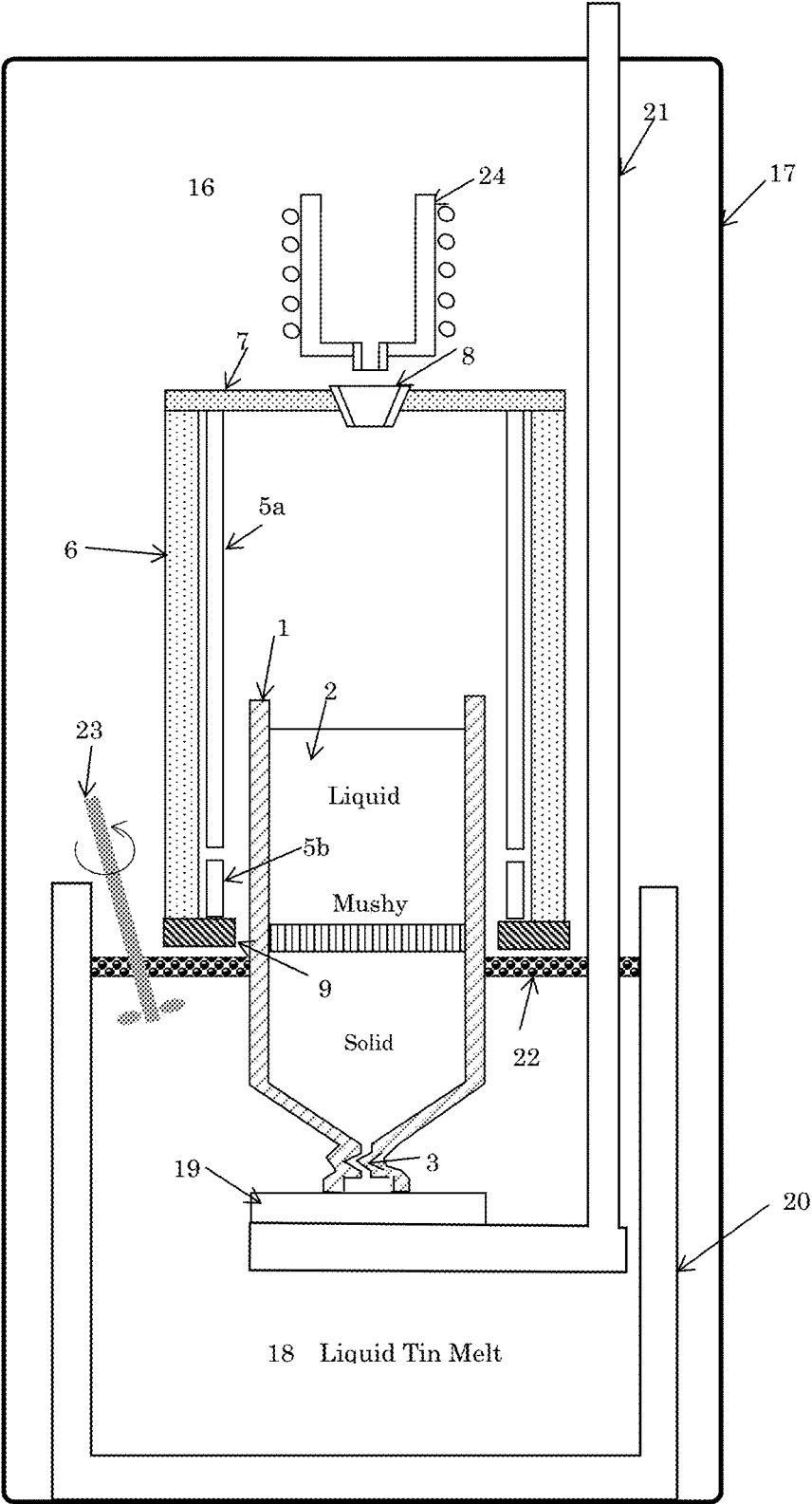
This invention is concerned with the production of directionally solidified castings or ingots to eliminate casting defects such as macrosegregation and misoriented grain defects that occur in the blades for jet engines and industrial gas turbines. The mechanism of the occurrence of the above casting defects was clarified by the computer simulation system developed by this inventor, and it was found that, by strongly cooling the solid phase region and applying an axial static magnetic field, the heat pulses at the solidification interface due to convection of the liquid phase can be suppressed, and harmful lateral liquid flow in the solid-liquid coexisting phase can be suppressed by the synergistic effect of these two measures. This eliminates casting defects such as macrosegregation and misoriented grain defects, also refines the microstructure to produce high-quality products with excellent mechanical properties (creep strength). Regarding the strength of the static magnetic field, it was found that there is a range where the macrosegregation becomes minimum in a relatively low magnetic field range. This makes it possible to keep the required magnetic strength low, which significantly reduces the price of expensive superconducting coils. In addition, productivity can be improved by increasing the withdrawal speed.

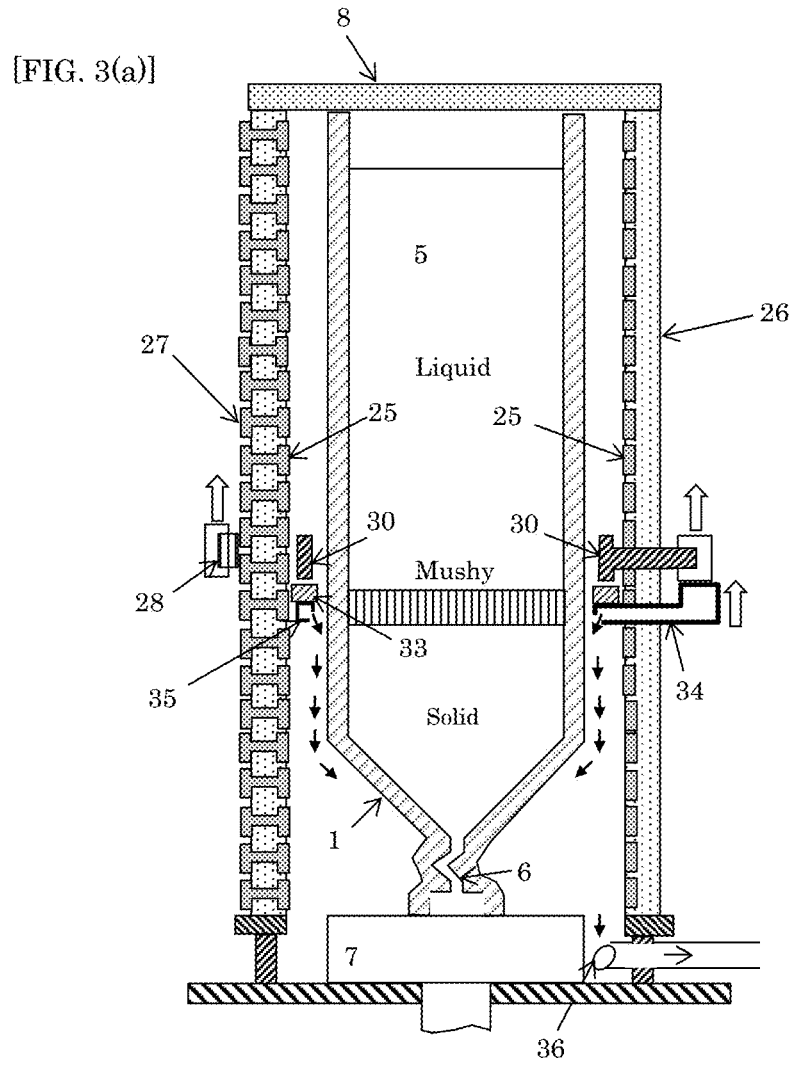


[FIG. 1]



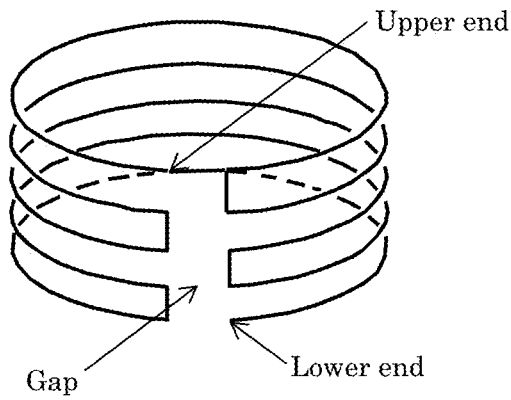
[FIG. 2]



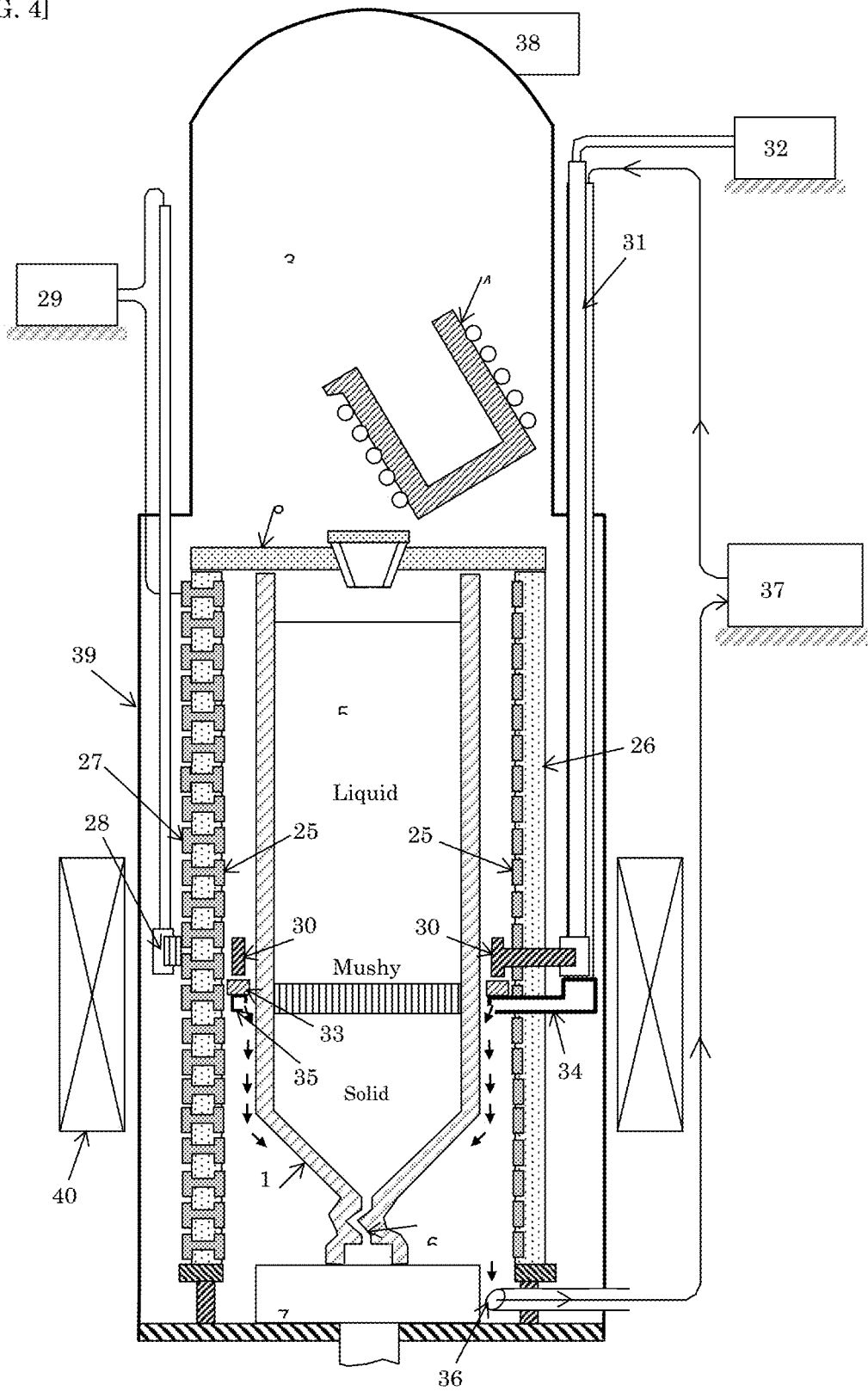


[FIG. 3(b)]

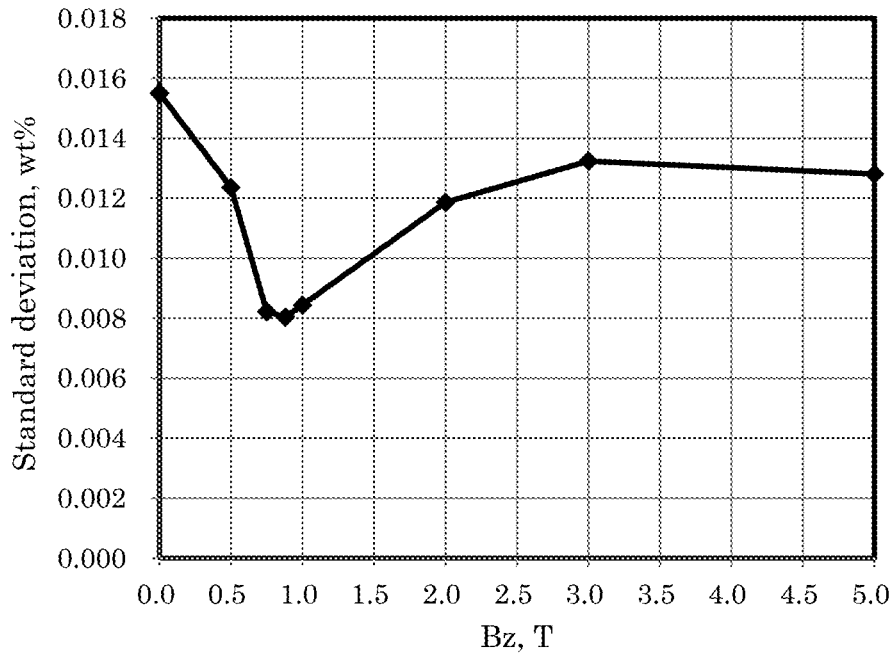
Main resistance heater 25



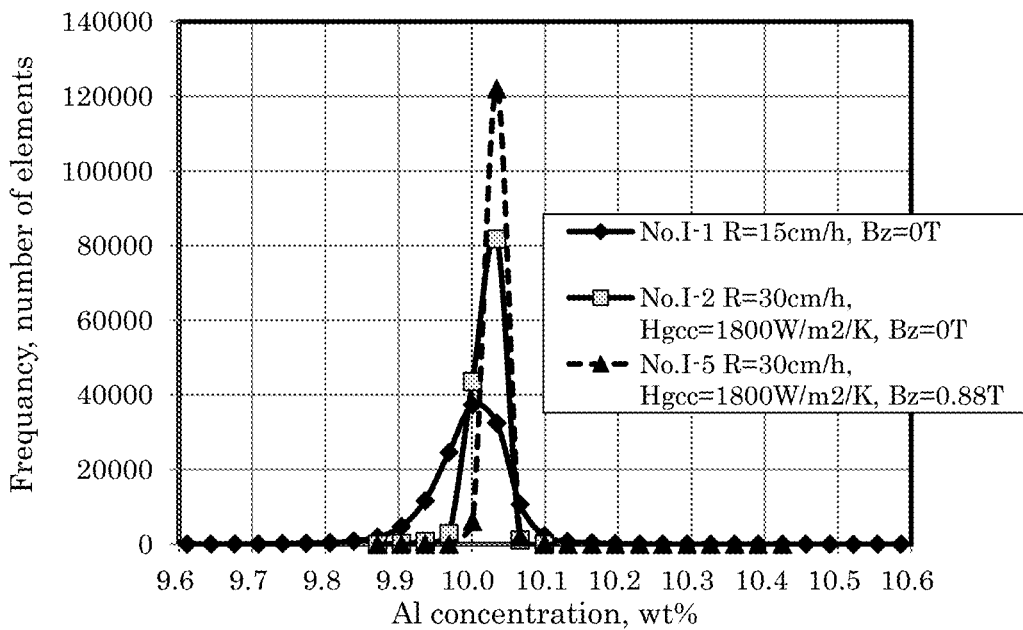
[FIG. 4]



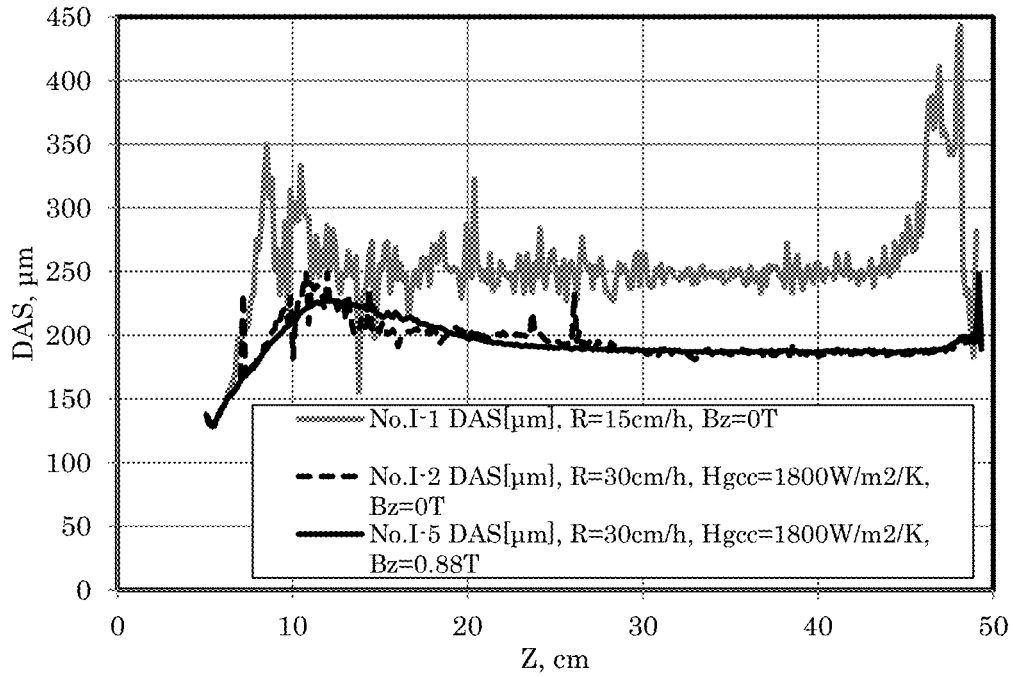
[FIG. 5]



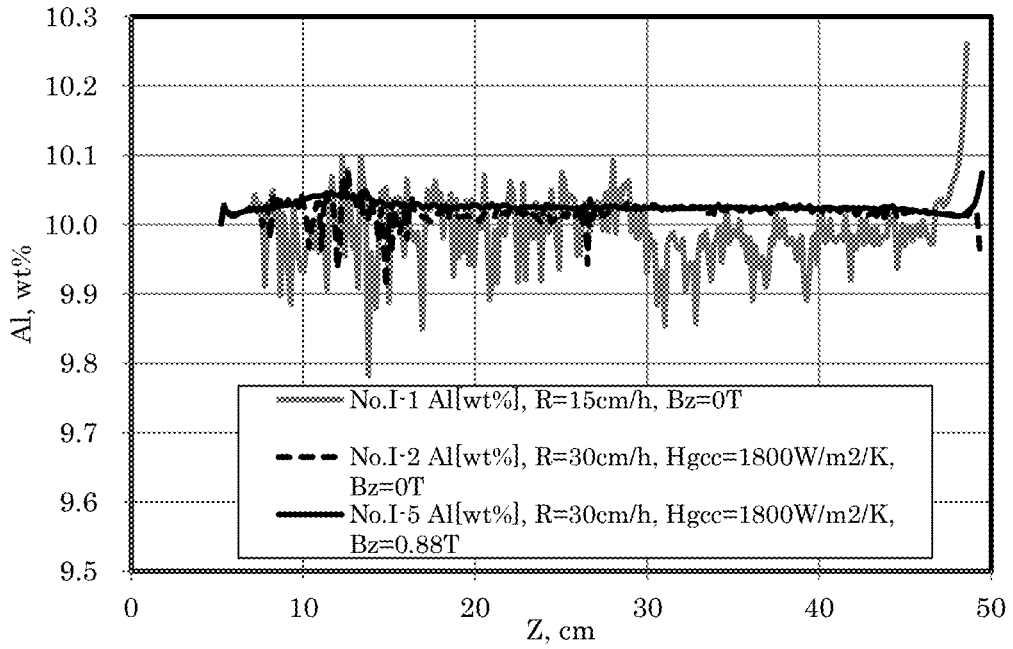
[FIG. 6]



[FIG. 7(a)]

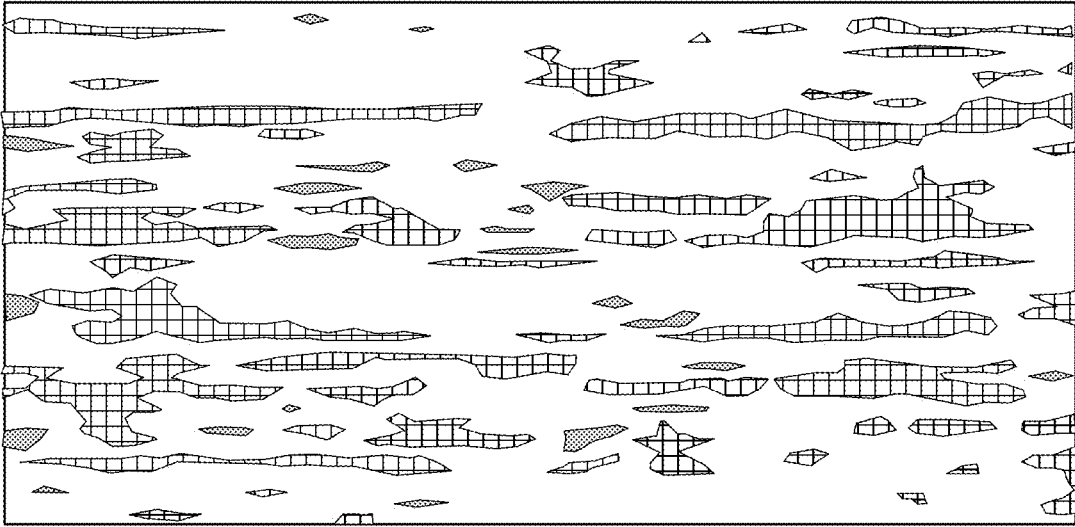


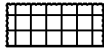


[FIG. 7(b)]



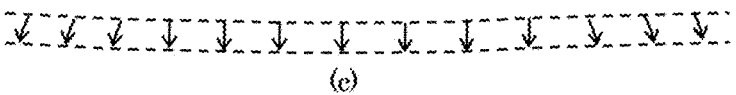
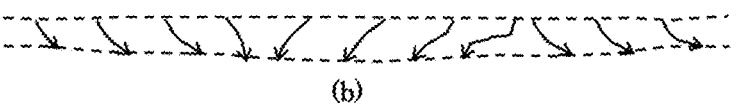
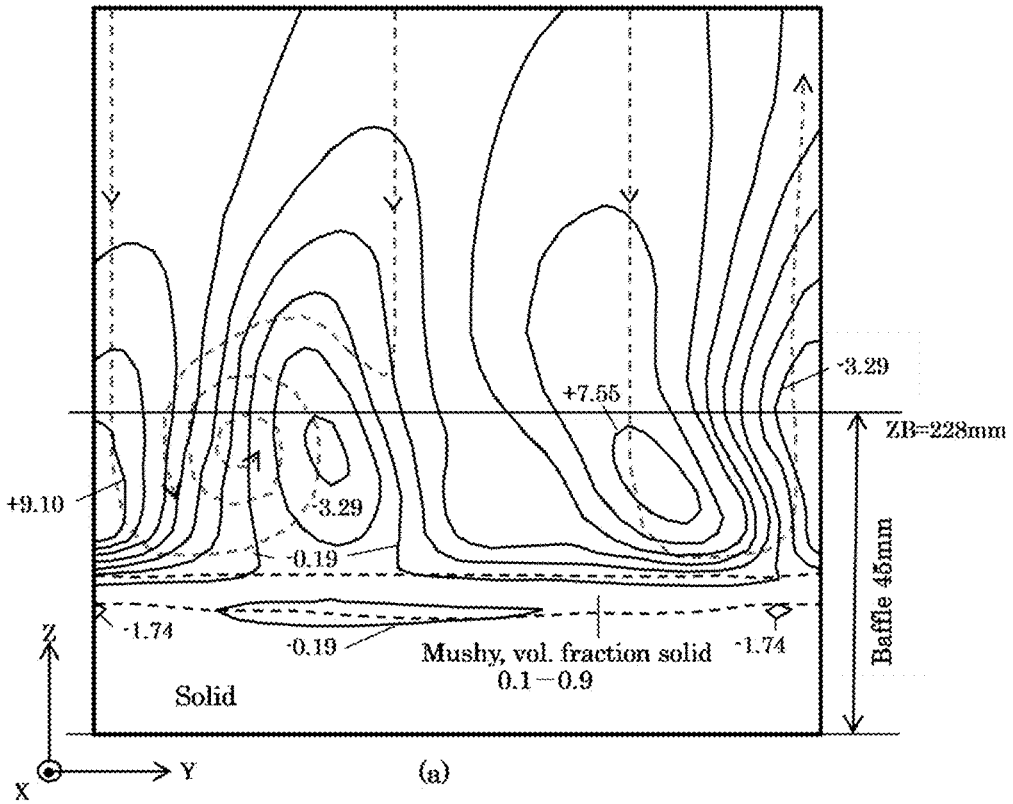
[FIG. 8]

No.I-1, Withdrawing speed 15 cm/h: Longitudinal section at the center of thickness direction, height 50mm, width 100mm

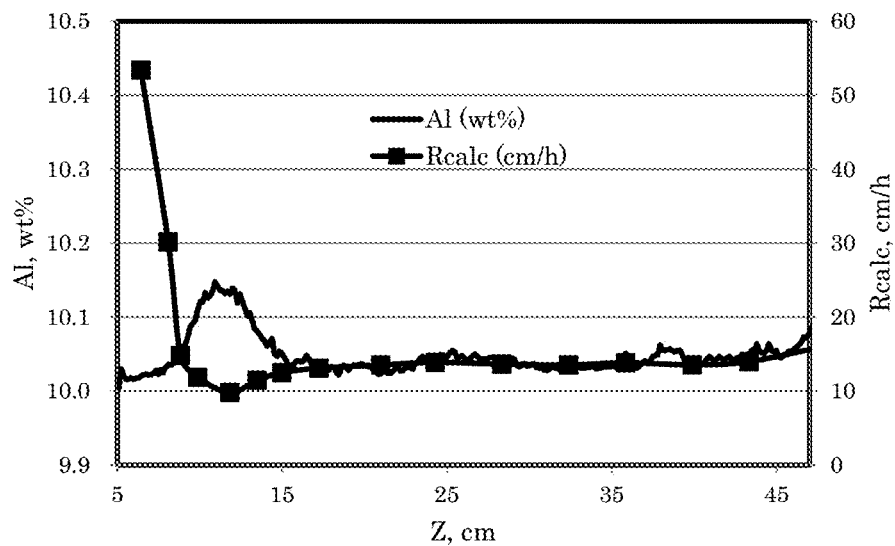


-  10.027 – 10.129 positive segregation
-  9.823 – 10.027
-  9.721 – 9.823 negative segregation

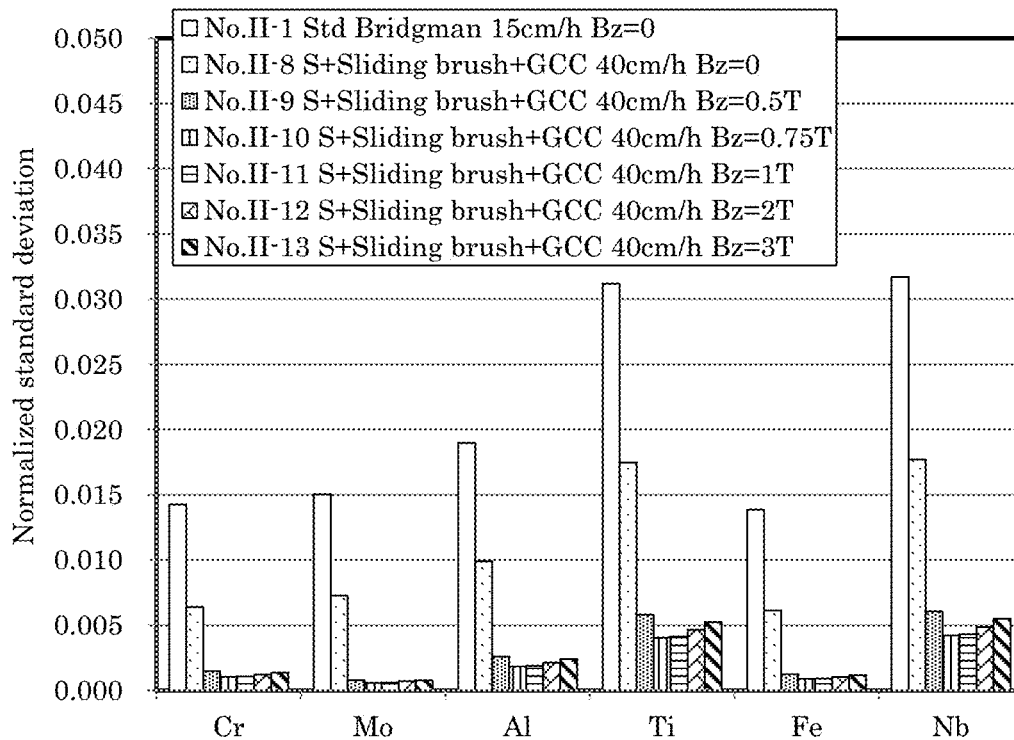
[FIG. 9]



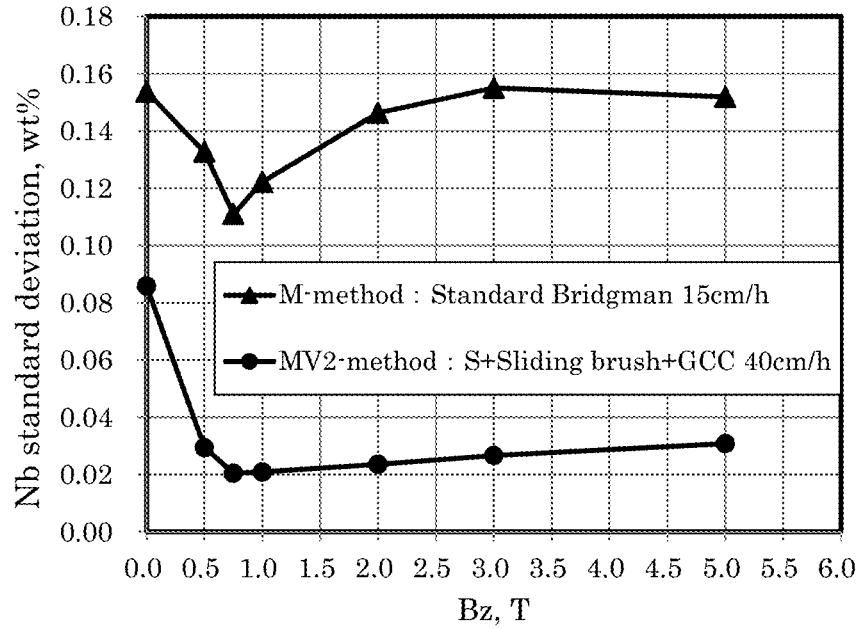
[FIG. 10]



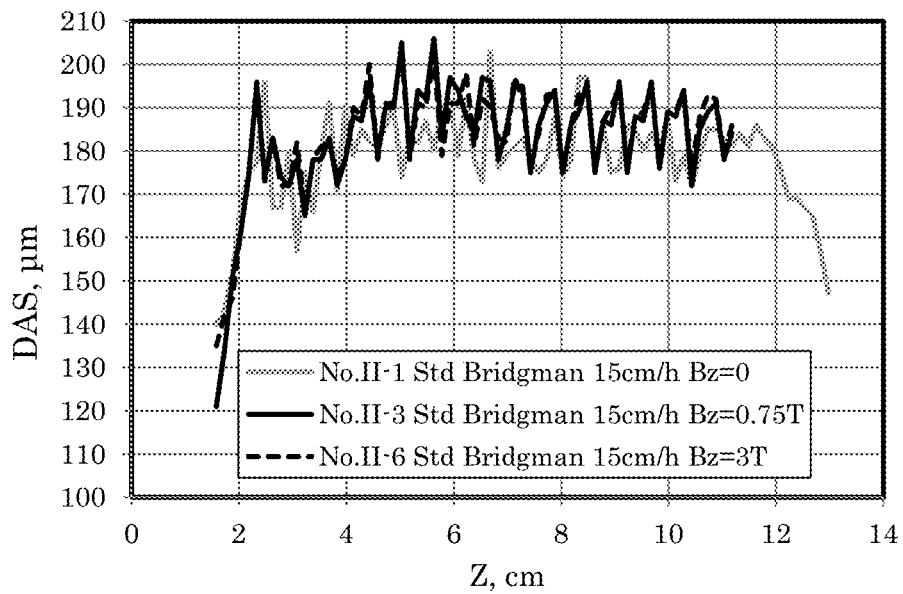
[FIG. 11]



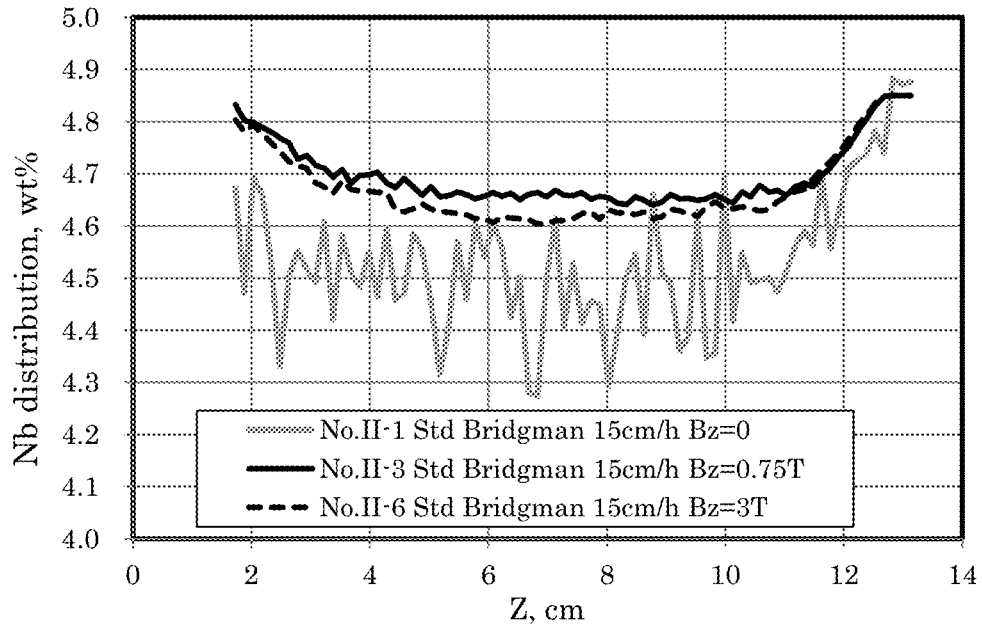
[FIG. 12]



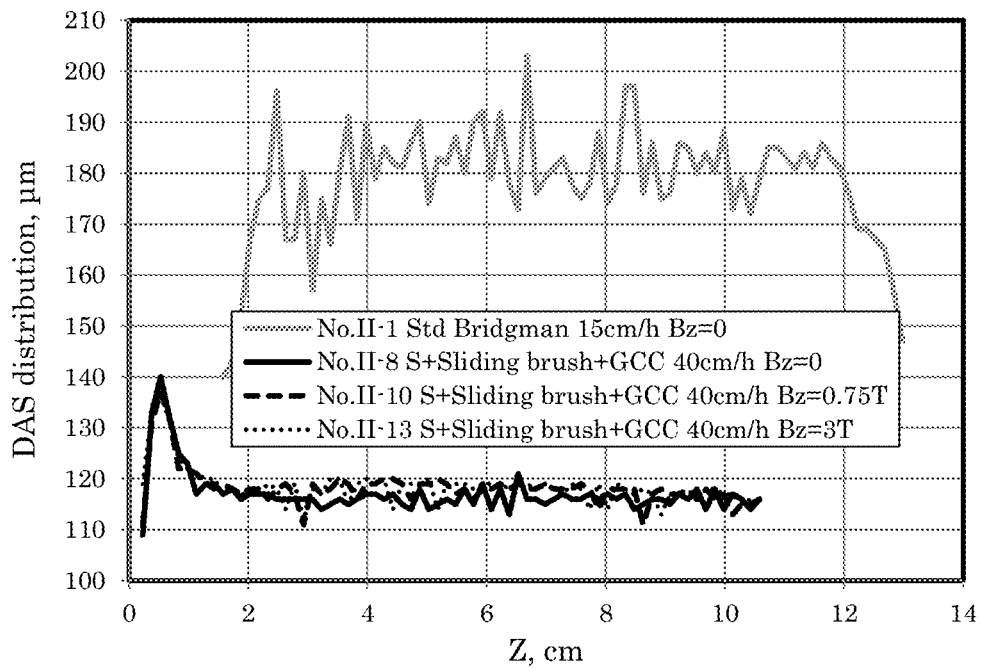
[FIG. 13]



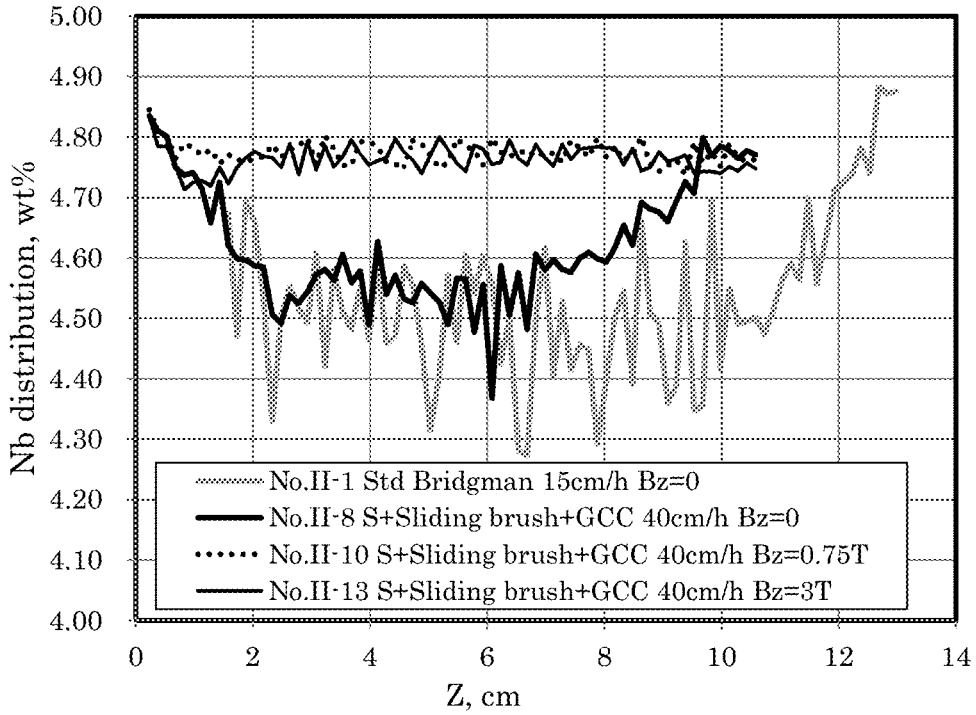
[FIG. 14]



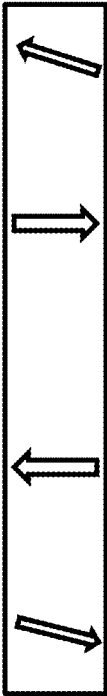
[FIG. 15]



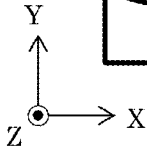
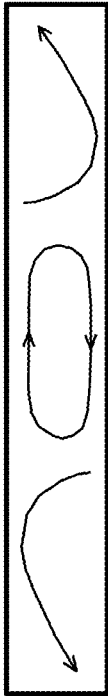
[FIG. 16]



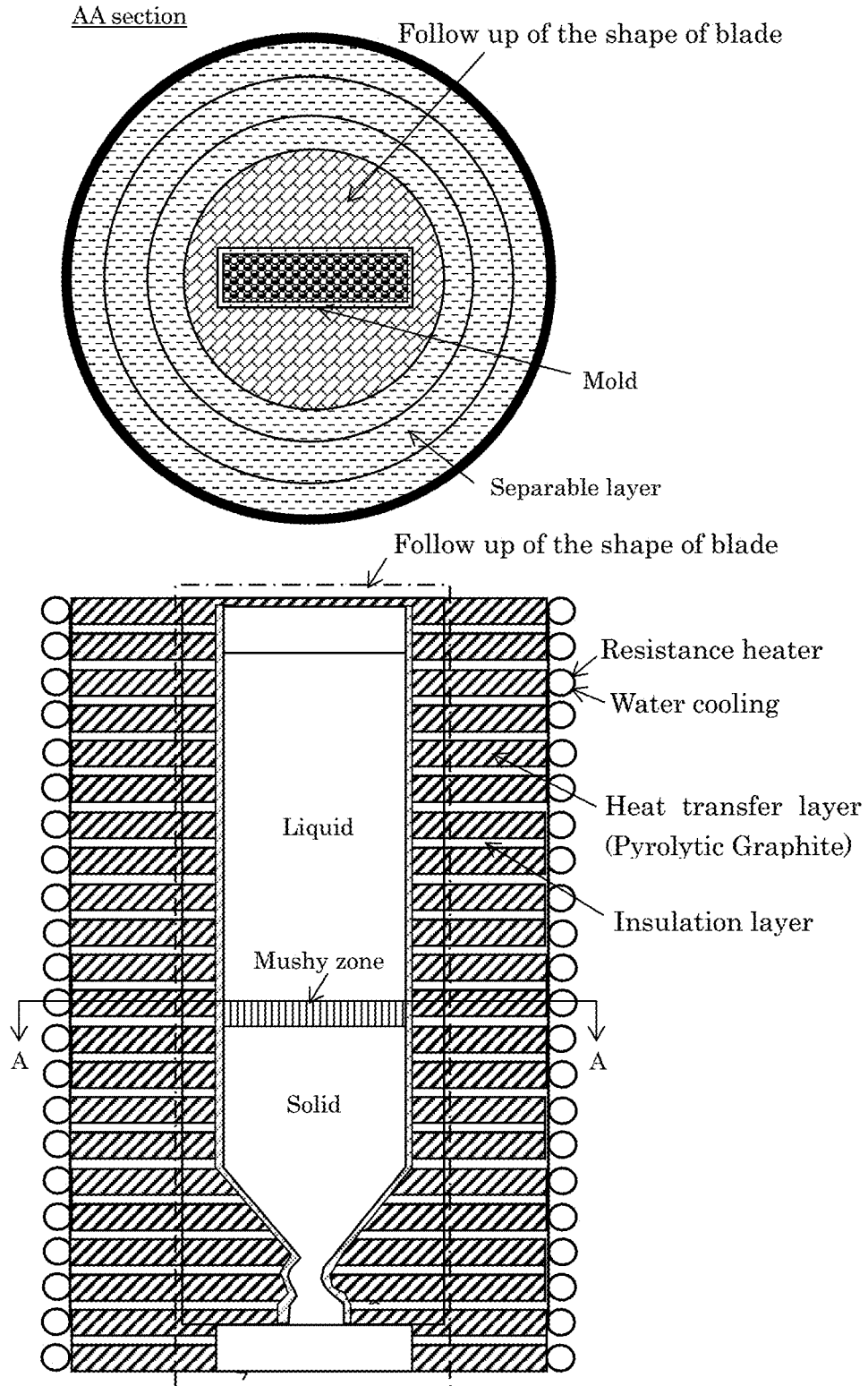
[FIG. 17(a)]



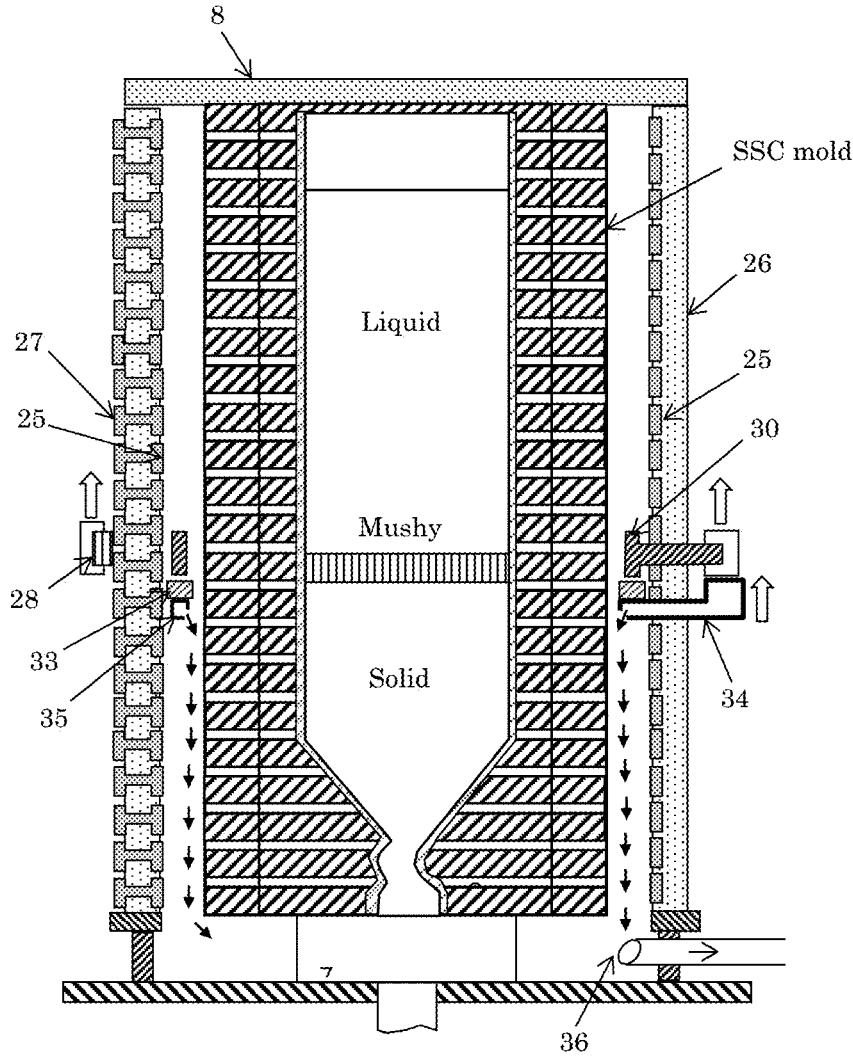
[FIG. 17(b)]

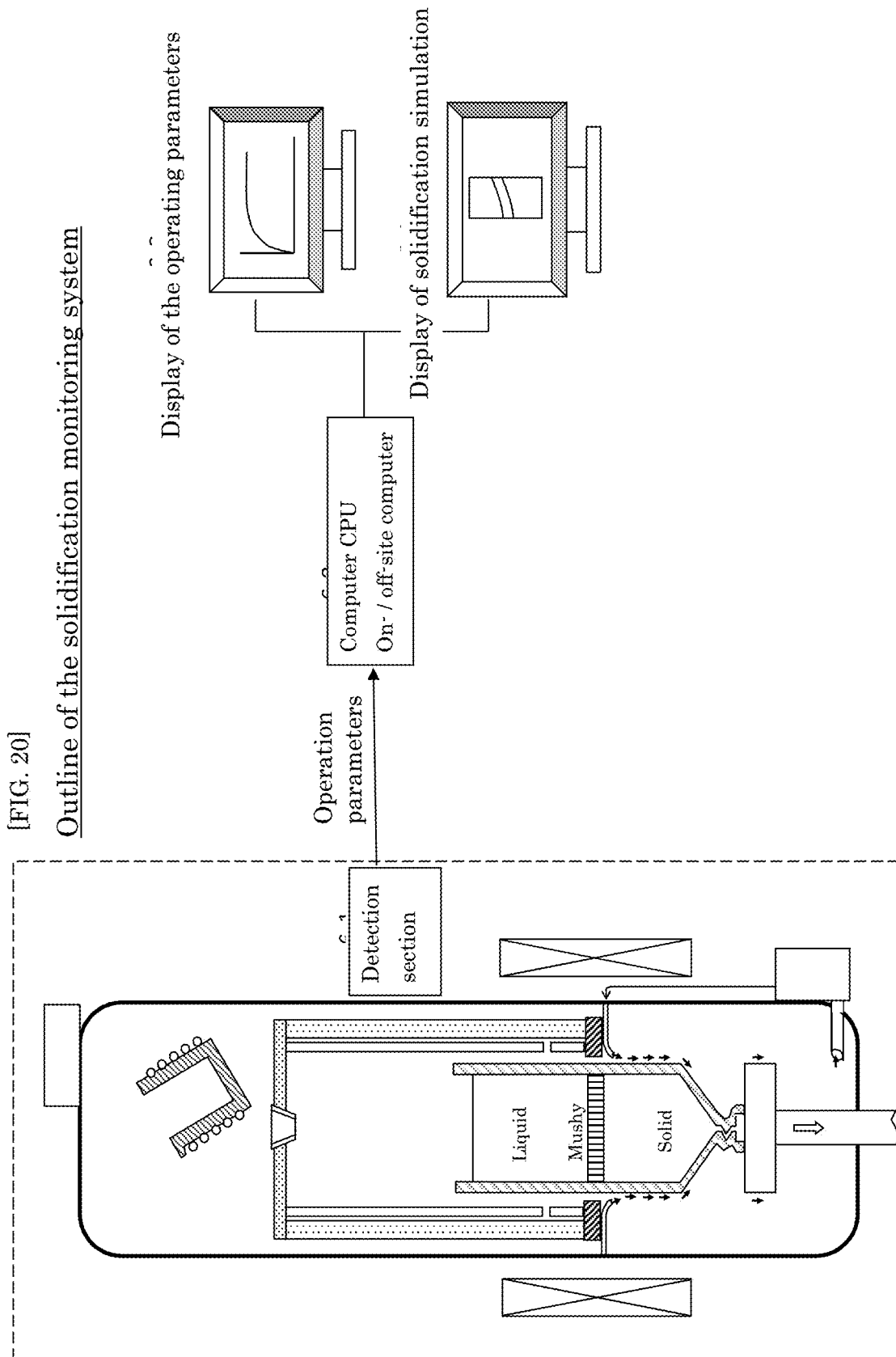


[FIG. 18]



[FIG. 19]





**UNIDIRECTIONAL SOLIDIFICATION
DEVICE, UNIDIRECTIONAL
SOLIDIFICATION METHOD,
UNIDIRECTIONALLY SOLIDIFIED
CASTING, AND UNIDIRECTIONALLY
SOLIDIFIED INGOT**

TECHNICAL FIELD

[0001] This invention is concerned with improved directional casting apparatus, directional casting method, and directional castings in the production of columnar dendrite structure consisting of polycrystalline grains (so called DS material) or dendrite structure consisting of a single crystalline grain (so called Monocrystal or SX material).

BACKGROUND ART

[0002] Bridgman method, Liquid Metal Cooling method, and Gas Cooling Casting method have been conventionally known as typical manufacturing methods for DS and SX materials. The outlines of these methods will be described below.

Bridgman Method

[0003] The apparatus of a typical Bridgman method (referred to herein as Standard Bridgman method) consists of a heating furnace, a cooling chamber, a mechanism for withdrawing a mold from the heating furnace to the cooling chamber, an adiabatic baffle that separates the heating furnace and the cooling chamber, and a cooling chill that initiates solidification (see, for example, Non-Patent Reference 1).

The mold is preheated above the melting temperature by a resistance heater, and after the pouring of the molten metal the mold is withdrawn into the cooling chamber at a prescribed speed. The mold is set on the cooling chill to start solidification by heat conduction to the chill. However, the effective cooling range by the chill is relatively short, and in the case of a large casting, its range is limited to the height of a grain selector (refer to FIG. 1). (Non-Patent Ref. 2 by Konter et al).

[The standard Bridgman method is of the one removing the cooling gas pump system 13 and the superconducting coil 14 from FIG. 1] The casting is solidified by radiation cooling in the cooling chamber. As will be described later, the cooling capability of radiation is quite small, so casting defects such as freckles (a type of macrosegregation defect that causes early failure of turbine blades) and misoriented grain defects are likely to occur. (For example, see p. 321 of Non-Patent Reference 1). These casting defects will be referred to in Paragraph 0029 below.

Liquid Metal Cooling Method (Hereinafter Referred to as LMC Method)

[0004] In order to eliminate the above-mentioned drawbacks of the standard Bridgman method, instead of radiation cooling, a method of cooling by immersing in a molten metal bath with low melting point was devised (hereafter referred to as Liquid Metal Cooling method, or LMC method). In the LMC method, the mold is gradually immersed in a low-melting-point molten metal bath such as tin or aluminum in the process of withdrawing the mold, thereby cooling the mold with increased cooling intensity, and thereby directionally solidifying the casting.

[0005] For example, U.S. Pat. No. 6,276,433B1 (2001) uses an Al eutectic alloy as a medium for cooling metal bath (Patent Reference 1). Furthermore, Elliott et al. (Non-Patent Reference 3) have shown that by using molten Sn with lower melting point than Al eutectic alloy as a cooling medium, it is possible to increase the cooling rate during solidification and improve the quality of Ni-based alloy turbine blades. In addition, Liu et al. (Non-Patent References 4 and 5) have adopted the LMC method and shown that the microstructure can be refined and the high temperature creep strength of directionally solidified Ni-based superalloy can be increased (For example, the creep rupture time at 1050° C. and 160 Mpa was approximately doubled from 84 hrs to 131 hrs. See Non-Patent Reference 5).

[0006] An example of a typical apparatus for the LMC method is shown in FIG. 2 (Non-Patent Reference 3). The heating area is equipped with upper and lower heaters (reference symbols 5a and 5b). The mold 1 is gradually immersed and cooled in the molten metal bath 18 by the mold withdrawal arm 21. A molten metal vessel 20 containing and holding the molten metal bath 18 adjusts the temperature of the metal bath by circulating hot oil therein. A heat insulating layer 22 made of floating alumina beads is provided on the surface of the molten metal bath 18 to block radiant heat from the heating area. The molten metal bath 18 is agitated by an agitator 23 to make the temperature uniform.

Gas Cooling Casting Method (Hereinafter Referred to as GCC Method)

[0007] An outline of the GCC method is shown in FIG. 1 (the superconducting coil 14 is excluded). The GCC method employs a forced gas cooling method in which inert gas (argon, helium, etc.) is used to intensely cool the mold pulled out into the cooling area (refer to Non-Patent Reference 2 and Patent Reference 2).

In FIG. 1, a cooling gas injection nozzle 11 for blowing a cooling gas is arranged immediately below the heat insulation baffle 9 provided to thermally separate the heating region and the cooling region, and during the directional solidification, the mold is cooled by blowing the inert gas onto it.

As an example of the cooling gas nozzle, an appropriate number of ejection ports are provided to eject swirling flow obliquely downward. The cooling gas blown out into the furnace is circulated by the gas pump system 13 along a path of suction/filtering/cooling/supply/suction to cool the mold in the cooling region.

According to the above reference, it is possible to obtain a cooling intensity equal to or higher than that of the LMC method.

[0008] However, even by the LMC method or the GCC method, it is not possible to eliminate the harmful liquid flow (turbulent flow) that inevitably exists in the bulk liquid zone and the solid-liquid coexisting zone (so-called mushy zone). Thus, it is difficult to completely eliminate macrosegregation or misoriented grain defects. In fact, the casting yield of large single-crystal blades for power generation is extremely low and has not been put to practice.

PRIOR ART REFERENCES

Patent References

[0009] [Patent Reference 1] U.S. Pat. No. 6,276,433B1 (2001)

[0010] [Patent Reference 2] U.S. Pat. No. 5,921,310 (Filed Sep. 26, 1997)

[0011] [Patent Reference 3] Japanese Patent 5,109,068

Non-Patent References

[0012] [Non-Patent Reference 1] ASM Handbook, Vol. 15, Casting (1988), p. 320, FIG. 3 or p. 321, FIG. 4

[0013] [Non-Patent Reference 2] M. Konter, et al: "A Novel Casting Process for Single Crystal Gas Turbine Components", Superalloy 2000, TMS 2000, p. 189

[0014] [Non-Patent Reference 3] A. J. Elliot et al: "Directional Solidification of Large Superalloy Castings with Radiation and Liquid-Metal Cooling", Metallurgical and Materials Transactions A, Vol. 35A, October, 2004, pp 3221-3231

[0015] [Non-Patent Reference 4] Lin Liu, et al: "The Effects of Withdrawal and Melt Overheating Histories on the Microstructure of a Ni-based Single Crystal Superalloy", TMS Superalloy 2008, pp 287-293

[0016] [Non-Patent Reference 5] Lin Liu, et al: "High Thermal Gradient Directional Solidification and its Application in the Processing of Ni-based Superalloys", J. Materials Processing Technology 210 (2010), pp. 159-165

[0017] [Non-Patent Reference 6] Y. Ebisu: 'A Numerical Method of Macrosegregation Using a Dendritic Solidification Model, and Its Applications to Directional Solidification via the use of Magnetic Fields', Metallurgical and Materials Transactions B, vol. 42b (2011), pp. 341-369

[0018] [Non-Patent Reference 7] M. C. Flemings: "Solidification Processing", McGraw-Hill, Inc., (1974)

[0019] [Non-Patent Reference 8] P. C. Carman: Trans. Inst. Chem. Eng., Vol. 15 (1937), p. 150

[0020] [Non-Patent Reference 9] Y. Fautrelle, et al: 'Thermo-Electric-Magnetic Hydrodynamics in Solidification: In Situ Observations and Theory', JOM, Vol. 70 (2018), No. 5, pp. 764-771

[0021] [Non-Patent Reference 10] X. Li, et al: 'Influence of thermoelectric effects on the solid-liquid interface shape and cellular morphology in the mushy zone during the directional solidification of Al—Cu alloys under a magnetic field', Acta Materialia, Vol. 55 (2007), pp. 3803-3813

[0022] [Non-Patent Reference 11] H. Zhong, et al: 'Effect of interdendritic thermoelectric magnetic convection on evolution of tertiary dendrite during directional solidification', J. Crystal Growth, Vol. 439 (2016), pp. 66-73

[0023] [Non-Patent Reference 12] J. Yu, et al: 'Influence of Axial Magnetic Field on Microstructures and Alignment in Directionally Solidified Ni-based Superalloy', ISIJ International, Vol. 57 (2017), No. 2, pp. 337-342

[0024] [Non-Patent Reference 13] W. Xuan, et al: 'Formation Mechanism of Stray Grain of Nickel-Based Single Crystal Superalloy Under a High Magnetic Field During Directional Solidification', Metall. Materi. Trans. B, Vol. 50B (2019), pp. 2019-2027

[0025] [Non-Patent Reference 14] Y. Lian, et al: 'Static Solid Cooling: A new directional solidification technique', J. Alloys and Compounds, Vol. 687 (2016), pp. 674-682

Outline of Invention

Problems to be Solved by Invention

[0026] In the production of DS or SX castings or ingots, even if the above-mentioned LMC method or GCC method

is applied, which has a higher cooling capability than that of the standard Bridgman method, it is difficult to essentially eliminate macrosegregation such as freckles or misoriented grain defects. In particular, the casting yield of large-sized SX blades for power generation is very low and are not put into practical use. The reason for this is that, as will be described later in Specific Examples, the lateral temperature gradient that inevitably exists in the liquid zone causes convection, brings heat pulses onto the solidification interface, influences the shape of the mushy zone, and disturbs the flow pattern of the liquid phase in the mushy zone. As a result, macrosegregation occurs. Furthermore, dendrite branches may separate and seed misoriented crystals. These tendencies would become stronger as the heat pulses increase.

Means for Solving Problems

[0027] To solve the above problems in these conventional methods,

[0028] (1) thickness of the mushy zone in axial direction is thinned by strongly cooling the solid zone and simultaneously increasing the withdrawal speed, so as to suppress the harmful lateral liquid flow within the mushy zone, and

[0029] (2) an axial static magnetic field is applied to suppress the convection in the liquid zone.

Synergistic effect of the above (1)+(2) eliminates the harmful heat pulses and suppresses the harmful lateral liquid flow within the mushy zone that causes macrosegregation. In doing so, the required magnetic field strength can be kept considerably low. The above findings are theoretically and quantitatively clarified for the first time by the solidification simulations described later. Thus, the synergistic effect of (1)+(2) makes essential points of the present invention.

[0030] In the present description, the method of applying an axial static magnetic field to the standard Bridgman method (refer to Patent Reference 3 or Non-Patent Reference 6) is called M method (Magnetic process), and the method described in the above Paragraph 0013, which is the present invention, is called MV1 method (Magnetic process Version 1). In the MV1 method, forced gas cooling by conventional GCC method or molten metal bath cooling by LMC method may be used as a strong cooling means.

[0031] Furthermore, a new directional solidification method is proposed herein. Its outline is shown in FIGS. 3(a) and (b). The apparatus of the invention comprises a mold 1 filled with molten metal 5, a cooling chill 7 placed at the bottom of the mold, and a resistance heater 25 serving as the main heater for heating the mold. The apparatus also includes a sub-heater 30 for heating the mold which is movable and targets a relatively small area, and a movable cooling gas nozzle 35 for blowing cooling gas onto the mold 1.

[0032] The sub-heater 30 and the movable cooling gas nozzle 35 are ring-shaped and configured to be coaxially and integrally movable against the mold 1 from the cooling chill 7 side to the upper end side. The movable cooling gas nozzle 35 is configured to blow the cooling gas obliquely downward onto the outer surface of the mold. A heat insulating baffle 33 is arranged between the sub-heater 30 and the cooling gas nozzle 35. As shown in FIG. 3(b), the resistance heater 25 is formed by winding a belt-like resistance heating element about one turn in the circumferential direction, raising it, and then winding it in the opposite direction about

one turn, there by repeating this procedure. As a result, a slit-like gap is formed, through which the cooling gas introduction pipe 34, the heat insulating baffle 33, and the sub-heater 30 can move up and down.

[0033] The main heater 25 is made of a resistance heating element such as carbon graphite, and is attached inside a cylindrical heat insulating sleeve 26. Further, the main heater 25 is connected to sliding contact terminals 27 arranged at the outside of the heat insulating sleeve 26. Then, a sliding brush 28 is attached onto the contact terminals 27. Electric power can be supplied to the main heater 25 through the contact terminal 27 at the uppermost end and the sliding brush 28 at the current position as shown in the figure.

In this description, the above heating method is referred to as Variable Resistance Heating method.

[0034] At the start of operation, the brush 28 is positioned at the lower end so that the entire region of the mold is heated and held at a prescribed temperature higher than the melting point of the alloy. The molten metal is poured and solidification commences at the chill. Then, the brush 28 is slid upward at a prescribed speed together with the cooling gas nozzle 35 and the sub-heater 30 so that solidification proceeds upward. Thus, as time passes, the heating zone shrinks and the cooling zone expands. Finally, the heating zone disappears, and the entire zone becomes a cooling zone to end the operation, and to finish the solidification.

[0035] FIG. 4 illustrates a schematic diagram incorporating the above devices. Reference symbol 29 is a power supply of the main heater, which supplies electric power through the upper end contact terminal 27 and the sliding brush 28. The sub-heater copper cable 31 connects the sub-heater power supply 32 and the sub-heater 30 to supply power. 38 is a vacuum pump, and 40 is a superconducting coil.

[0036] The cooling gas pump system 37 supplies the cooling gas to the cooling gas nozzle 35 through the cooling gas inlet pipe 34, and the suction port 36 is an intake port for circulating cooling gas blown into heat insulating sleeve 26. The cooling gas is circulated along a path of suction/filtering/cooling/supply/suction. The melting chamber 3 containing the induction melting furnace 4 and the mold chamber containing the mold 1 can be separated, and after solidification the mold is taken out. This DS method is called MV2 method (Magnetic process Version 2: S+sliding brush+GCC+Bz, S means single chamber).

Effects of the Invention

[0037] The synergistic effects are obtained based on the MV1 method or MV2 method as follows.

[0038] (1) During solidification, the heat pulses brought onto the solidification interface due to convection in the liquid zone are eliminated so that the solidification becomes stabilized, and the lateral flow in the mushy zone is suppressed (i.e., rectified in the axial direction). As a result, macrosegregation is suppressed and the occurrence of the misoriented grain defects is suppressed. [It is well known that macrosegregation does not take place when the liquid flow within the mushy zone is rectified in the axial direction (see, for example, p. 252 of Non-Patent Reference 7, FIGS. 7-35)]

[0039] (2) As will be described later in the Specific Examples, the required static magnetic field strength can be greatly reduced compared with the simple

M-method, leading to a significant cost down of the expensive superconducting coils.

[The price of a superconducting coil is determined by the superconducting material, bore size and magnetic field strength. Since the price is highly dependent on the magnetic field strength, it is one of the key objectives of the present invention to keep the magnetic field as low as possible.] In addition, the productivity can be increased by increasing the withdrawal speed.

[0040] (3) Compared with the standard Bridgman method or the simple M method, much stronger cooling intensity can be obtained, so as described in Paragraph 0005, which makes it possible to obtain fine microstructures of Ni-based superalloy blades.

Then, an economical merit is obtained by shortening required time for solution treatment. And at the same time, it becomes possible to produce a product with high creep rupture strength (refer to Non-Patent Reference 5).

BRIEF DESCRIPTION OF DRAWINGS

[0041] FIG. 1 is a schematic drawing showing an embodiment of a directional solidification apparatus by the present invention (referred to as MV1 method).

[0042] FIG. 2 shows an example of a directional solidification apparatus by the LMC method.

[0043] FIG. 3 (a) is a schematic diagram showing the outline of the directional solidification apparatus using a sliding electrode system by the present invention, and (b) shows the main resistance heater of (a).

[0044] FIG. 4 is a schematic diagram showing an example of the sliding electrode system (referred to as MV2 method). Shown are vacuum chamber 3, induction melting furnace 4, cooling gas circulation system 37 and magnetic coils 40 for applying an axial static magnetic field onto the mushy zone.

[0045] FIG. 5 shows the effect of axial static magnetic fields on Al segregation standard deviations of Ni-10 wt % Al blade by MV1 method (R=30 cm/h, H_{gcc}=1800 W/m²/K).

[0046] FIG. 6 shows Al segregation histograms of Ni-10 wt % Al blades by standard Bridgman method (R=15 cm/h) and MV1 method (R=30 cm/h, H_{gcc}=1800 W/m²/K).

[0047] FIG. 7 (a) shows the effects of the axial static magnetic fields on the DAS distributions of Ni-10 wt % Al blades by the standard Bridgman method (R=15 cm/h) and the MV1 method (R=30 cm/h, H_{gcc}=1800 W/m²/K). Cross-sectional center in Z direction). Note: bottom chill thickness is 4.5 cm.

[0048] FIG. 7 (b) shows the effects of the axial static magnetic fields on the Al distributions of Ni-10 wt % Al blades by the standard Bridgman method (R=15 cm/h) and the MV1 method (R=30 cm/h, H_{gcc}=1800 W/m²/K). Cross-sectional center in Z direction). Note: bottom chill thickness is 4.5 cm.

[0049] FIG. 8 shows a schematic diagram showing the morphology of Al macrosegregation of Ni-10 wt % Al blade by the standard Bridgman method (longitudinal section at the center of thickness direction).

[0050] FIG. 9 (a) shows a schematic diagram of the heat pulses due to convection in front of the solidification interface of Ni-10 wt % Al large-sized blade by Standard Bridgman method (No. I-1: R=15 cm/h, 1/2 solidified, longitudinal section at the center in thickness direction). The heat pulses (or thermal fluctuation) is shown by T1±dT K at time step t-dt to t (t=5469 s, dt=2s) with 10 contours

between Max+10.65 K and Min -4.84 K. Broken lines with arrows denote stream lines. Two broken lines in horizontal direction denotes mushy zone. ZB is the height from the bottom of the blade to the baffle,

[0051] (b) shows the flow pattern within the mushy zone denoted by the two broken lines in horizontal direction of Figure (a), No. I-1, and

[0052] (c) shows the flow pattern within the mushy zone when MV1-method is applied (No. I-6: R=30 cm/h, $\frac{1}{2}$ solidified, t=2877 s, longitudinal section at the center in thickness direction).

[0053] FIG. 10 shows the relationship between the moving speed R_{calc} of solidification interface (calculated value) and the Al distribution of the Ni-10 wt % Al large-sized blade (simple M method by standard Bridgman, withdrawal speed 15 cm/h, $B_z=1T$).

[0054] FIG. 11 shows the effects of the axial static magnetic fields on normalized segregation standard deviations of IN718 blades by the MV2 method (GCC, sliding brush 40 cm/h). The standard deviations of each elements (Table 7) are normalized by initial alloy contents. S in the figure denotes single chamber.

[0055] FIG. 12 shows the effects of the axial static magnetic fields on Nb segregation standard deviations of IN718 blades by the simple M method (standard Bridgman, withdrawal speed 15 cm/h) and MV2 method (GCC, sliding brush 40 cm/h). S in the figure denotes single chamber.

[0056] FIG. 13 shows the effects of the axial static magnetic fields on DAS distributions of the IN718 blades (Z direction at cross-sectional center) by the simple M method (standard Bridgman, withdrawal speed 15 cm/h). Note: Bottom chill thickness=1.5 cm. For No. II-3 and No. II-6, the calculations of the upper parts of the blades were omitted because of the formation of shrinkage.

[0057] FIG. 14 shows the effects of the axial static magnetic fields on Nb distributions of the IN718 blades by the simple M method (standard Bridgman, withdrawal speed 15 cm/h, cross-sectional center, Z direction). Note: Bottom chill thickness=1.5 cm. For No. II-3 and No. II-6, the calculations of the upper parts of the blades were omitted because of the formation of shrinkage.

[0058] FIG. 15 shows the effects of the axial static magnetic fields on DAS distributions of the IN718 blades by the MV2 method (GCC, sliding brush 40 cm/h, cross-sectional center, Z direction). Note: Dummy chill thickness=0.15 cm (from Table 6). No. II-1 is the result of the standard Bridgman.

[0059] FIG. 16 shows the effects of the axial static magnetic fields on Nb distributions of the IN718 blades by the MV2 method (GCC, sliding brush 40 cm/h, cross-sectional center, Z direction). Note: Dummy chill thickness=0.15 cm (from Table 6). No. II-1 is the result of the standard Bridgman.

[0060] FIG. 17 (a) shows schematic diagrams of the Lorentz force vectors and (b) the flow pattern within the mushy zone induced by the axial static magnetic field (MV2 method, No. II-10, GCC, sliding brush 40 cm/h, $B_z=0.75T$).

[0061] FIG. 18 shows a schematic diagram of the Static Solid Cooling method (see Non-Patent Reference 14).

[0062] FIG. 19 shows a schematic diagram of a mold design by the Static Solid Cooling method adopted in the directional solidification apparatus by the MV2 method of the present invention (however, the heating and cooling

means depend on those of the present invention. The overall design including magnetic coils is omitted for brevity).

[0063] FIG. 20 shows an overview of a directional solidification monitoring system by the MV1 method (and MV2 method) of the present invention.

BEST MODE FOR CARRYING OUT THE INVENTION

[0064] In the MV1 method or MV2 method of the present invention, the cooling rate during solidification is increased and the solidified structure is refined as compared with the simple M method. Furthermore, casting defects such as macrosegregation or misoriented crystals have been eliminated, and at the same time, the required static magnetic field strength has been reduced, thereby making it possible to reduce the cost of superconducting coils.

SPECIFIC EXAMPLES

A. Mechanism for the Formation of Macrosegregation

[0065] It is well known that various macrosegregations, including Freckle segregation, are caused by liquid flow within the mushy zone. Solidification contraction, convection due to the density difference in the interdendritic liquid phase, and external forces such as electromagnetism force contribute as the driving forces to cause this flow.

Since the density of interdendritic liquid phase during solidification is expressed as a function of the alloy concentrations in the liquid phase and temperature T, it is given by

$$\rho_L = \rho_L(C_1^L, C_2^L, \dots, T) \quad (1)$$

(Refer to the formula to calculate liquid density in Table 3). In the formula, C denotes alloy concentration, lower subscript numbers 1, 2, . . . denote alloys, and upper superscript L denotes liquid phase.

[0066] An alloy in which ρ_L decreases as solidification proceeds is called upward type of buoyancy, on the other hand, an alloy in which ρ_L increases is called downward type of buoyancy. It depends on the alloy compositions whether it is an upward type, a downward type, or a mixed type (i.e., ρ_L decreases first and increases again with the progress of solidification, or vice versa). Ni-10 wt % Al is an upward type alloy, and IN718 is a downward type alloy (see FIG. 13 of Non-Patent Reference 6).

[0067] For example, in an alloy containing Al (where Al is lighter than Ni), the concentration of Al is increased as solidification proceeds, so that the density of the interdendritic liquid phase becomes relatively smaller than the density of initial liquid phase. Therefore, when such an alloy is solidified in the direction opposite to the gravity, the density of the liquid phase at the root of the dendrites, becomes relatively smaller compared with that of the liquid phase at the tip of the dendrites. Such alloys are referred to herein as 'solute unstable' against convection.

[0068] On the other hand, from a view point of temperature distribution, the temperature is lower at the root of the dendrites than at the tip, and therefore denser at the root so that convection does not occur. That is, it is 'thermally stable'. When the solute instability is greater than the thermal stability, a density inversion layer is formed, and the liquid phase in the mushy zone tends to generate ascending convection so that so-called chimney type freckles are likely to occur. Macrosegregation with such morphology is likely to occur in upward-type alloys. However, regardless of

upward, downward or mixed type of buoyancy, it exhibits various forms depending on the casting conditions.

[0069] In addition, heat pulses caused by convection bring about dendrite re-melting/separation (called the grain multiplication mechanism; see p. 154 of Non-Patent Reference 7), which would break the growth of dendrites, leading to misoriented grain defects with random crystallographic orientations. B Effect of Suppressing Liquid Metal Flow by Static Magnetic Field

[0070] It is known that when a temperature gradient exists in the solid and liquid phases of metals (good electrical conductors), a thermoelectric current is generated in the direction of the temperature gradient (so-called Seebeck effect). Using Ohm's law, the current field is expressed as follows.

$$J = \sigma(-\nabla\varphi - S/T) \quad (2)$$

(Note: S has a negative value for Ni-based alloys. See Table 3) where J is the current density vector (A/m²), σ is the electrical conductivity (1/ Ω m), φ is the electric potential (V), S is the Seebeck's coefficient or thermoelectric power (V/K), ∇T is the temperature gradient vector (K/m). The second term on the right side of the equation is a contribution term due to the thermoelectric current by S. Furthermore, taking into account the current density $\sigma(\mathbf{V} \times \mathbf{B})$ induced by the flow velocity vector V of the liquid phase (or solid phase) and the externally applied static magnetic field vector B, Eq. (3) is obtained.

$$J = \sigma(-\nabla\varphi - S\nabla T + \mathbf{V} \times \mathbf{B}) \quad (3)$$

From the continuity condition of the current field,

$$\nabla \cdot \mathbf{J} = 0 \quad (4)$$

The electromagnetic force (Lorentz force) f (N/m³) produced by J and B is given by the following equation.

$$\mathbf{f} = \mathbf{J} \times \mathbf{B} \quad (5)$$

Substituting Eq. (3) into Eq. (4) yields the following equation for φ .

$$\nabla \cdot (\sigma \nabla \varphi) = -\nabla \cdot (\sigma S \nabla T) + \nabla \cdot (\sigma \mathbf{V} \times \mathbf{B}) \quad (6)$$

φ is obtained by solving Eq. (6), J is obtained by Eq. (3), and then the Lorentz force f can be calculated from Eq. (5). However, V must be calculated by the numerical analysis which includes momentum equation where the flow field and the electromagnetic field have a highly coupled relationship. f is included in the body force term of the momentum equation. The electrical boundary condition at the blade-mold boundary (including the blade-cooling chill boundary) were assumed insulated.

[0071] Here, some Non-Patent literature will be reviewed which take into account the thermoelectromagnetic force. Fautrelle, et al (Non-Patent Reference 9) have applied a static magnetic field of 0.08T in the thickness direction (horizontal direction) to an Al—Cu alloy of a width 5 mm×height 5 mm×thickness 200 μ m and performed X-ray in-situ observation during solidification. Then, it has experimentally been shown that the liquid phase or the solid phase moves due to the Lorentz force generated even by as low a magnetic field of 0.08T for the temperature gradient in the height direction.

[0072] Non-Patent Reference 10 has applied a static magnetic field during the DS cellular growth process of an Al—Cu alloy (3 mm in diameter×200 mm in length) and shown that convection due to the thermoelectromagnetic

force affects the cellular morphology. That is, a ring-shaped cellular structure was formed by a weak magnetic field of 0.5T or less (see FIG. 6 of the reference).

[0073] Non-Patent Reference 11 investigated the effects on dendrite morphology by applying an axial static magnetic field in the DS dendrite growth process of Al-4.5 wt % Cu alloy using <001> oriented 4 mm diameter seed crystal. The results showed that the tertiary branches grow unevenly like windmills when magnetic fields higher than 2T are applied (see FIGS. 2 and 3 in the Reference). Then, presetting a dendritic configuration model where one dendrite crystal with cross-shaped secondary branches is placed in a cylinder of a diameter 100 μ m×height 250 μ m, a numerical simulation has been performed with TEM force GS VT and EM braking force $\sigma(\mathbf{V} \times \mathbf{B}) \times \mathbf{B}$ considered, showing that the convections occur around the primary trunk in the planes perpendicular to the growth direction, and develop the windmill-like tertiary branches (For reference, the typical flow velocity at that time is about 25 μ m/s = 2.5×10^{-3} cm/s, the growth rate is 50 μ m/s = 5×10^{-3} cm/s, and $B_z = 6T$ (refer to FIGS. 7 and 8 of the Reference).

[0074] Non-Patent Reference 12 has shown that, when an axial static magnetic field higher than 2T is applied in the DS process of Ni-based superalloy DZ417 alloy (specimen diameter 4 mm×length 180 mm), columnar dendrites break down to yield an equiaxed grain structure. This tendency becomes more pronounced as the withdrawal speed, i.e., the growth rate is slowed down and the magnetic field is increased (see FIGS. 2 and 3 of the Reference).

[0075] Non-Patent Reference 13 used a seed crystal 15° tilted in advance with respect to the axial direction in the DS Ni-based superalloy single crystal PWA1483 alloy (sample diameter 4 mm×length 130 mm), and a static magnetic field was applied in the axial direction (withdrawal speed = 50 μ m/s = 18 cm/h). The results showed that when no magnetic field was applied, no misoriented grain defects (stray grains) occurred, but that when a high magnetic field of $B_z = 5T$ was applied, stray grains occurred on the outer periphery of the sample (refer to FIGS. 1 (c) and (d) of the Reference).

[0076] All the above references show that the driving force $\sigma S \nabla T \times \mathbf{B}$ induced by thermal current and static magnetic field brings about the convection and affects the morphology of dendrites. However, they do not refer to the effect on macrosegregation.

[0077] On the other hand, the purpose of the present invention is to clarify the mechanism for the formation of macrosegregation by a rigorous computer simulation on solidification assuming real directional solidification process of Ni-based alloys, and, as described in Paragraph 0013, to clarify the means for eliminating the macrosegregation defect by applying static magnetic field.

C. Method of Solidification Analysis

[0078] The outline of a general-purpose simulation system (named CPRO™ of EBIS Corporation, Sagami, Japan) for solidification is described below which has been developed by the present inventor to analyze solidification phenomena. The physical variables to be analyzed are the temperature, the solute concentrations of alloying elements redistributed in the liquid and solid phases during solidification (the number of alloying elements is n), liquidus temperature giving the relationship between the temperature and volume fraction solid, and liquid flow vectors and pressure in the liquid and mushy phases. These variables are

referred to herein as the macroscopic variables. These n+6 variables and their corresponding governing equations are listed in Table 1.

TABLE 1

Relationship between physical variables and governing equations (n is the number of alloying elements)	
Physical variables	Governing equations
Temperature	Energy eq.
Solute concentrations in liquid	Solute redistribution eqs. of n alloys (Solute mass conservation law)
Liquidus temperature	Temperature vs volume fraction solid eq. of multi-alloy system
Liquid flow vectors	Momentum eqs. (Darcy's law included)
Pressure of liquid	Pressure eq.
Number of variables is n + 6	Number of equations is n + 6

[0079] It is known that the flow in the mushy zone is described by Darcy's equation (7) (refer to p. 234 of Non-Patent Reference 7). The Darcy's flow is included as flow resistance terms in the momentum equations.

$$v = \frac{K}{\mu g_L} (-\nabla P + X) \quad (7)$$

Here, the vector V denotes the interdendritic liquid flow velocity, μ the viscosity of liquid, g_L the volume fraction liquid, K the permeability, P the pressure of liquid phase, and X the body force vectors such as gravity or centrifugal force. Note that X also includes the thermoelectromagnetic driving force and the electromagnetic braking force introduced in the present invention. K is determined by the geometrical structure of dendrites and is given by the Kozney-Carman equation below (refer to Non-Patent Reference 8s).

$$K = \frac{(1 - g_s)^3}{5S_b^2} \quad (8)$$

S_b is the surface area per unit volume of the dendrite crystals (called specific surface area), and is determined by morphological analysis during the growth of the dendrite crystals (the scale is microscopic). Since solidification is regarded as a kind of diffusion rate-controlled process in the liquid and solid phases, the dendrite is modeled with cylindrical branches and a trunk and hemispherical tips, and the solute diffusion equation in the solid and liquid phases are solved to obtain S_b (refer to Appendix B of Non-Patent Reference 6). g_s the volume fraction solid. K is assumed isotropic. The value of the dimensionless number 5 in the formula was determined by flow experiments in porous media.

[0080] Furthermore, the influences of the thermoelectromagnetic driving force and the electromagnetic braking force due to the static magnetic field were incorporated into the aforementioned numerical solution. This allows a complete description of the solidification phenomena taking these forces into account. It was assumed that the solid phase in the mushy zone is stationary. When a uniform static magnetic field Bz is applied only in the axial direction, the Lorentz forces acting on the bulk liquid zone and the liquid phase in the mushy zone are specifically written down as follows.

$$f_x = -\sigma \frac{\partial \phi}{\partial y} Bz - \sigma S \frac{\partial T}{\partial y} Bz - \sigma V_x B_z^2 \quad (9)$$

$$f_y = \sigma \frac{\partial \phi}{\partial x} Bz + \sigma S \frac{\partial T}{\partial x} Bz - \sigma V_y B_z^2 \quad (10)$$

$$f_z = 0 \quad (11)$$

(S has negative values for Ni-based alloys)

It can be seen that these body forces act only in lateral directions, not in the axial direction (Z-direction).

[0081] As mentioned above, since all the physical variables on the macroscopic scale are interacting with each other, and are deeply related to the dendrite growth on the microscopic scale (that is, both scales are coupled), an iterative convergence method was employed to obtain the solution. This numerical method is described in detail in the present inventor's paper (Non-Patent Reference 6).

Specific Example 1

Ni-10 wt % Al Long Blade by Standard Bridgman Method

[0082] As an example of the present invention, the effect of MV1 method (strong cooling+axial magnetic field) will be described below by computer simulations of plate ingot simulating the manufacture of Ni-10 wt % Al turbine blade. [By preliminary simulations, it was found that the results were substantially the same whether or not a seed crystal (thickness of 5 mm, initial temperature of 300° C.) is used. Therefore, the results are valid for both cases] In the MV1 method, the GCC method was used as a strong cooling means. Table 2 shows the casting parameters used for the calculation, and Table 3 shows the chemical composition and physical properties.

[0083] Konter et al. (Non-Patent Reference 2) have shown that when using the GCC method, the cooling performance can be enhanced by optimizing the angle of the cooling gas nozzle installed directly under the heat insulating baffle and the distance between the nozzle and the mold surface (See FIG. 8 in the Reference). That is, for $q=HGCC$ (ceramic mold surface temperature-ambient temperature), HGCC can be increased up to

$$H_{GCC}=1000-2000 \text{ W/(m}^2\cdot\text{K)} \quad (12)$$

$H_{GCC}=1800 \text{ W/(m}^2\cdot\text{K)}$ in Table 2 was set considering this effect.

[0084] Casting parameters of Ni-10 wt % Al blade are given in Table 2

TABLE 2

Casting parameters of Ni-10 wt % Al alloy large-sized blade (M-method)
Dimensions: 18 mm thickness × 100 mm width × 470 mm height
Element partition: Blade part is equally partitioned, 2 mm in X dir., 1.5 mm in Z dir., 2 mm in Y dir.
Mold thickness (ceramic mold): 10 mm
Baffle height: 45 mm
Withdrawal rate: 2.5 mm/min (15 cm/h) and 5 mm/min (30 cm/h)
Casting temperature: 1753 K (1480 C.) (superheat 80 K)
Initial temperature of mold: 1723 K
Initial temperature of chill: 573 K
Radiation heat exchanges between mold and heater (heating zone) and between mold and inner surface of furnace (cooling zone): I.D. of the heater and I.D. of the furnace in the cooling chamber were both set to

TABLE 2-continued

Casting parameters of Ni-10 wt % Al alloy large-sized blade (M-method)

300 mm diameter, and the heating zone and the cooling zone were assumed insulated by the baffle (height 45 mm). Defining Q_{ig} as the radiation heat exchange between the 'i'-th element on the mold surface and the 'g'-th element either on the inner surface of the heater or the inner surface of the furnace (cooling chamber) or the mold surface itself, the radiant heat exchange of the 'i'-th element is expressed by

$$Q_i = \sum_{g=1}^{g_{max}} Q_{ig} = \sum_{g=1}^{g_{max}} \frac{\sigma(T_i^4 - T_g^4)}{\frac{1 - \epsilon_i}{\epsilon_i} + \frac{1}{F_{ig}} + \frac{A_i}{A_g} \frac{1 - \epsilon_g}{\epsilon_g}}$$

where g_{max} is the total number of 'g' elements.
 σ : Stefan-Boltzmann constant
 T_i : Surface temperature of the mold
 T_g : Surface temperature of heater or inner surface temperature of the furnace in the cooling zone or surface temperature of the mold itself
 Temperature of the heater = 1773 K, the furnace in the cooling zone = 400 K
 ϵ_i : Emissivity of the mold surface = 0.35
 ϵ_g : Emissivity of the heater or inner surface of furnace in the cooling zone or the mold surface
 $\epsilon_g =$ Emissivity of the heater = 0.3
 $\epsilon_g =$ Emissivity of the inner surface of the furnace = 0.4
 A_i : Area of the mold surface element i
 A_g : Surface area corresponding to A_i (the heater or the inner surface of the furnace or the mold surface itself)
 F_{ig} denote view angles which require a very large memory. So, an algorithm to save the memory has been employed (refer to J. Yu et al; J. Mater. Sci. Technol., vol. 23 (2007), p. 47-54).

TABLE 2-continued

Casting parameters of Ni-10 wt % Al alloy large-sized blade (M-method)

Forced gas cooling of mold surface by GCC method (refer to Non-Patent Reference 2):
 $q = H_{GCC} (T_m - T_o) + Q_i$ (W/m^2) (q includes the above Q_i)
 Heat transfer coefficient by cooling with inert gas $H_{GCC} = 1800$ $W/(m^2 \cdot K)$
 T_m : Mold surface temperature
 T_o : Atmospheric temperature in cooling zone 400 K
 Heat flux due to air gap formation at ingot-mold boundary (refer to Non-Patent Reference 2):

$$q = \frac{\sigma(T_1^4 - T_2^4)}{\frac{1}{\epsilon_1} + \frac{1}{\epsilon_2} - 1} \quad (W/m^2)$$

***applied in the cooling zone.
 T_1 : Surface temperature of the solid
 T_2 : Inner surface temperature of the mold
 ϵ_1 : 0.4 Emissivity on the surface of the solid
 ϵ_2 : 0.35 Emissivity on the inner surface of the mold
 Heat flux at ingot -chill boundary: $q = h (T_{i1} - T_{c2})$ (W/m^2)
 h : Heat transfer coefficient 418 $W/(m^2 \cdot K)$
 T_{i1} : Ingot temperature at the bottom
 T_{c2} : Chill temperature at the upper surface
 Water cooling at the bottom of chill: $q = h (T - T_w)$ (W/m^2)
 h : Heat transfer coefficient 84 $W/(m^2 \cdot K)$ (Assumed)
 T : Chill temperature at the bottom
 T_w : Water temperature 293 K

[0085] Chemical compositions and physical properties of Ni-10 Al and IN718 alloys are given in Table 3

TABLE 3

Chemical compositions and physical properties of Ni-10Al and IN718 alloys						
	Cr	Mo	Al	Ti	Fe	Nb
Ni-10Al (wt %)			10.0			
IN718 (wt %)	19.0	3.05	0.55	0.90	19.40	4.85
Liquidus and solidus curves of Ni-Al phase diagram are non-linear as below:						
Temperature (C.)		1453	1430	1420	1405	1385
Liquid composition (wt %)		0	5.15	7.2	10.05	12.9
Solid composition (wt %)		0	4.17	5.85	8.2	10.9

Constants in liquid density equation $\rho_L = \rho_0^L + \sum_n h_n C_n^L + h^0 T_L$:

The values of these constants are determined from the densities for pure liquid metals (refer to T. Iida and R. L. L. Guthrie: The physical properties of liquid metals, Clarendon Press, Oxford, UK, 1993, pp. 70-73)

Alloy	ρ_0^L (g/cm^3)	h_0 (g/cm^3C)	h_n ($g/cm^3 \cdot wt\%$)					
			Cr	Mo	Al	Ti	Fe	Nb
Ni-10Al	9.380	-1.05×10^{-3}			-0.0871			
IN718	9.453	-1.022×10^{-3}	-0.0145	0.0242	-0.0953	-0.0587	-0.0089	0.0029

Physical properties of specific surface area of dendrite, Sb (refer to Eq. (28) of Non-Patent Reference 6):
 Configuration factor of dendrite: $\phi = 0.67$ for cylinder
 Surface energy at solid-liquid interface, σ_{LS} (cal/cm^2):
 6×10^{-6} for Ni-10Al; 5×10^{-5} for IN718
 Correction factor α of Sb: 0.6 for IN718; 0.4 for Ni-10Al

TABLE 3-continued

Chemical compositions and physical properties of Ni-10Al and IN718 alloys							
Diffusion coefficients	Ni-10Al		IN718				
	Al	Cr	Mo	Al	Ti	Fe	Nb
in liquid D^L (cm ² /s)	1.0×10^{-4}	Assumed to be 2.3×10^{-5} for all elements in reference to the data given by P. N. Quedsted and M. Maclean: Mater. Sci. Eng., 1984, vol. 65, pp. 171-84.					
Specific heat of liquid (cal/g/C.)		Ni-10Al	IN718	Bottom plate	Shell mold: Specific heat = 0.20		
Specific heat of solid (cal/g/C.)		0.15(*)	0.15(*)	(dummy):	Specific Thermal conductivity =		
Thermal conductivity (cal/cm/s/C.)		0.15(*)	0.15(*)	heat = 0.15	0.036(Non-Patent Ref		
Liquid		0.064(*)	0.064(*)	Thermal conductivity =	2)		
Solid		0.064(*)	0.064(*)	Density=7.4	Density=1.7		
Solid density in mushy zone(g/cm ³)		7.4	7.94				
Density of solid(g/cm ³)		7.4	7.95				
Latent heat of fusion (cal/g)		50.0	50.0				
Viscosity of liquid (poise)		0.05	0.07(*)				
Surface tension of liquid (dyn)		920.0	920.0(*)				

(*) These are assumed in reference to the data given by M. C. Schneider, et al.: Metall. Mater. Trans. A, 1997, vol. 28A, pp. 1517-31
 For Ni-based superalloys, Sl and Ss of 10 wt % Al and IN718 were approximated as follows from Table III of W. Xuan, et al., Metall. Mater. Trans. B, vol. 47B (2016), pp. 828-833:
 Thermoelectric power of liquid S_l (V/K) $S_l = (-6.897 \times 10^{-3} T - 5.655) \times 10^{-6}$ (T < 1773 K)
 Thermoelectric power of solid S_s (V/K) $S_s = (-5.943 \times 10^{-3} T - 5.779) \times 10^{-6}$ (T < 1673 K)
 Thermal properties Cu-chill:
 Specific heat (cal/g/C) = $2.222 \times 10^{-5} * T + 0.0915$ (0 < T < 200 C.)
 Specific heat (cal/g/C) = $2.6 \times 10^{-5} * T + 0.091$ (200 < T < 600 C.)
 Thermal conductivity (cal/cm/s/C) = $0.9554 - 1.222 \times 10^{-4} T$ (0 < T < 200 C.)
 Thermal conductivity (cal/cm/s/C) = $0.9595 - 1.425 \times 10^{-4} T$ (200 < T < 600 C.)
 Density = 8.0 (g/cm³)

[0086] The mold withdrawal speed was adjusted by preliminary calculation so that the position of the mushy zone was at approximately the same horizontal position as the insulating baffle. Thus, the withdrawal speed for the standard Bridgman method was set at R=15 cm/h, and for the GCC method at R=30 cm/h (and HGCC=1800 W/(m²·K)). The results were summarized in Table 4.

TABLE 4

Computational results of Ni-10 wt % Al large-sized blade (MV1-method)					
No. Specification	Standard deviation, wt %	Mean, wt %	Min-Max, wt %	Thermal fluctuation in front of solidification interface, K	
I-1 R = 2.5 mm/min, Bz = 0	5.146e-02	9.998	9.447-10.341	TI - 4.84 to TI + 10.65 at 5469 sec, time step = 2 s	
I-2 R = 5 mm/min, Bz = 0, HGCC = 1800W/m ² /K	1.553e-02	10.019	9.871-10.096	TI - 5.14 to TI + 4.68 at 2742 sec, time step = 2 s	
I-3 R = 5 mm/min, Bz = 0.5T, HGCC = 1800W/m ² /K	9.113e-03	10.028	9.936-10.125	No fluctuation	
I-4 R = 5 mm/min, Bz = 0.75T, HGCC = 1800W/m ² /K	8.222e-03	10.029	9.978-10.170	No fluctuation	
I-5 R = 5 mm/min, Bz = 0.88T, HGCC = 1800W/m ² /K	8.040e-03	10.030	9.985-10.095	No fluctuation	
I-6 R = 5 mm/min, Bz = 1T, HGCC = 1800W/m ² /K	8.440e-03	10.030	9.995-10.075	No fluctuation	
I-7 R = 5 mm/min, Bz = 2T, HGCC = 1800W/m ² /K	1.186e-02	10.030	9.993-10.119	No fluctuation	
I-8 R = 5 mm/min, Bz = 3T, HGCC = 1800W/m ² /K	1.324e-02	10.030	9.978-10.133	No fluctuation	

TABLE 4-continued

Computational results of Ni-10 wt % Al large-sized blade (MV1-method)				
No. Specification	Standard deviation, wt %	Mean, wt %	Min-Max, wt %	Thermal fluctuation in front of solidification interface, K
I-9 R = 5 mm/min, Bz = 5T, H _{GCC} = 1800W/ m ² /K	1.281e-02	10.031	9.978-10.138	No fluctuation

Note 1:

R is withdrawal rate and H_{GCC} is heat transfer coefficient by GCC method.

Note 2:

Thermal fluctuation is defined by $TI \pm dT$, where TI (1673 K) is liquidus temperature.

[0087] The standard deviation σ (wt %) (i.e., square root of the sum of the squares of the differences between the Al concentrations of each computational element and the average value) was used as an index for evaluating the degree of segregation. The larger the σ , the greater the variation of Al, i.e., the greater the degree of macrosegregation. While in the case of withdrawal speed $R=15$ cm/h, $\sigma=5.146E-02$ wt % (No. I-1), in the case of increased withdrawal speed $R=30$ cm/h plus stronger cooling with $H_{GCC}=1800$ W/m²/K, σ reduces to $1.553E-02$ wt % (No. I-2).

[0088] Furthermore, when an axial static magnetic field Bz is applied, σ changes as shown in FIG. 5. That is, when $Bz=0.88T$, it becomes the minimum value (No. I-5), and when Bz is increased in the region greater than 1T, σ reversely increases. This minimum value is the optimum solution for minimizing macrosegregation. However, it is not always necessary to set this optimum solution, but it is sufficient to adopt a magnetic field intensity close to the optimum value.

[0089] FIG. 6 is the corresponding histograms showing approximately normal distributions. It can be clearly seen that as σ decrease, the widths of the variations decrease. Also, the dendrite arm spacing (DAS) and Al concentration distributions in Z direction at cross-sectional center are shown in FIGS. 7(a) and 7(b), respectively. In the case of No. I-1, the $DAS \approx 250$ μ m and the variation width 30 μ m, whereas in No. I-5, the $DAS \approx 190$ μ m and the variation has almost disappeared. As for the Al macrosegregation, as shown in FIG. 7(b), almost no variation is observed in the optimum solution, compared with the variation of 9.95-10.05 wt % for the standard Bridgman (No. I-1).

[0090] A schematic diagram of Al macrosegregation is shown in FIG. 8. In this example, the freckles that often develop in the axial direction do not occur, but rather band-like macrosegregation extending roughly in horizontal directions is observed.

On the Solidified Structure

[0091] The cooling rate during solidification for the Standard Bridgman method is determined as $GR=46.9 \times 15 / 3600 = 0.2^\circ$ C./s from the temperature gradient in axial direction of 46.9° C./cm and the withdrawal speed of $R=15$ cm/h, similarly for the GCC method $GR=0.5^\circ$ C./s from $G=59.8^\circ$ C./cm, and corresponding dendrite arm spacing (DAS) become 250 μ m and 190 μ m, respectively. Thus, the solidification structure is refined. Application of a static magnetic field further reduces the variation widths, i.e., increases homogeneity. In the case of GCC, there is almost no

variation (see FIG. 7(a)). The reason why DAS is small at the bottom of the ingot is because, at the initial stage of solidification, the solidification rate increases due to the rapid cooling effect of the chill (that is, as shown in FIG. 10, the moving speed of solidification interface R_{calc} (calculated value) is initially fast, gradually decreases, passes through a minimum value, and settles at a constant value, i.e., the predetermined withdrawal speed of 15 cm/h)

Morphology of Macrosegregation and the Effect of Static Magnetic Field

[0092] A typical segregation pattern by the Standard Bridgman method has already been shown in FIG. 8 (longitudinal section at the center in thickness direction). Since other longitudinal section shows similar aspects, we will discuss the longitudinal section at the center in thickness direction as follows. The segregations repeat positive and negative (greater than or less than 10 wt % Al) in the longitudinal direction. Horizontal sections also show the same way, but the frequency of positive and negative segregation (number of repetitions) is less than that in the longitudinal direction. Such form is called "band segregation" or so-called "banding" in this description.

[0093] In the case of no magnetic field, the banding fluctuation becomes larger because the horizontal temperature gradient that inevitably exists in front of the solidification interface causes convection, which induces heat pulses at the interface and significantly changes the liquid flow pattern in the mushy zone. An example of the heat pulses is shown in FIG. 9(a) (Standard Bridgman method, no magnetic field). The heat pulses are expressed by contours of temperature variation at time step $t-\Delta t$ to t . The temperature near the solidification interface increased by a maximum of 10.65° C. due to the high-temperature downward flow from the top (outlined by the dashed lines), and the liquid phase cooled at the interface was cooled by a maximum of -4.84° C. on the return path ($\Delta t=2$ sec).

[0094] The mushy zone is constantly affected by these heat pulses, causing fluctuations in its temperature, volume fraction solid, dendrite morphology, shape of the mushy zone and ultimately the liquid flow pattern (see FIG. 9(b)). As a result, band-like macrosegregation (see FIG. 8) is formed.

[0095] When the axial magnetic field Bz was applied, convection in the bulk liquid zone disappeared, and heat pulses also disappeared (not shown for want of space). FIG. 9(c) shows a schematic diagram of the flow pattern within the mushy zone in the longitudinal section at the center in

thickness direction for No. I-3 (Bz=1T+strong cooling+high withdrawal speed). The figure shows that the width of the mushy zone becomes narrower and the lateral flow is decreased, and that the flow pattern tends to be rectified in the axial direction. As a result, the Al variation or macrosegregation is virtually eliminated as described above.

[0096] The maximum segregation in FIG. 10 can be explained so that the phenomenon hidden by the convection reappeared as the convection subsided by the application of Bz. It is known that, in DS, macrosegregation increases or decreases when the moving speed of the solidification interface suddenly accelerates or decelerates, respectively (for example, refer to p. 39, FIGS. 2-6; p. 40, FIGS. 2-7 of Non-Patent Reference 7). That is, at the initial transition stage of solidification, the change of Rcalc corresponds to the Al maximum, whose range is about 13 cm from the bottom. [The same applies to the change in DAS at the initial transition stage shown in FIG. 7(a).]

[0097] As mentioned above, the macrosegregation has been reduced to a level where there is no practical problem due to the synergistic effect of the forced cooling by GCC and the relatively low magnetic field less than 1T (i.e., by relatively low cost of superconductive coil). Furthermore, since heat pulses are eliminated and solidification is stabilized, misoriented grain defects should be suppressed. It also brings about advantages by refining the microstructure (i.e., increased creep rupture strength and reduced solution heat treatment time). Note that the discrepancy between computed values and the initial content in Table 4 is considered to be a background error generally associated with such complex numerical analysis.

Specific Example 2

IN718 Alloy Short Blade

[0098] Next, the simulations of Simple M method (Standard Bridgman method, R=15 cm/h+Bz) and MV2 method (S+sliding brush+GCC+Bz, R=40 cm/h) for the IN718 short blade will be described blow (S means Single chamber). Table 3 shows the physical properties of IN718, Table 5 shows the casting parameters by the Simple M method, and Table 6 shows the casting parameters according to MV2 method of the present invention. Preliminary computations were performed to adjust the casting parameters so that the position of the solid-liquid coexisting phase (mushy zone) was placed at approximately the same horizontal position as the insulating baffle: Thus, withdrawal speed R=15 cm/h for the M method and R=40 cm/h and HGCC =600 W/(m²·K) for the MV2 method.

[0099] The Tables 5 and 6 are shown as follows.

TABLE 5

Casting parameters of IN718 small-sized blade (M-method)
Dimensions: 6 mm thickness × 42 mm width × 120 mm height
Element partition: Blade part is equally partitioned, 1 mm in X dir., 1.5 mm in Z dir., 1.5 mm in Y dir.
Mold thickness (ceramic mold): 5 mm
Baffle thickness: 10 mm
Withdrawal rate: 2.5 mm/min (15 cm/h)
Casting temperature: 1673K (superheat 66K)
Initial temperature of mold: 1673K
Initial temperature of chill: assumed to be 1423 (solidus temperature) -293 = 1130 K. This is a measure to accelerate the timing of reaching steady state.

TABLE 5-continued

Casting parameters of IN718 small-sized blade (M-method)
Radiation heat exchanges between mold and heater (heating zone) and between mold and inner surface of furnace (cooling zone): I.D. of the heater and I.D. of the furnace were set to 92 mm, and the heating zone and the cooling zone were assumed insulated by the baffle (thickness 10 mm). Equations and parameters are same as those presented in Table 2 except for the following values.
Tg = 1693K (heater), Tg = 400K (inner surface of furnace)
εi: Emissivity of mold surface 0.35
εg: Emissivity of heater and inner surface of furnace: εg = 0.3 (heater), εg = 0.4 (inner surface of furnace)
Regarding the calculation of view angles Fig, the same algorithm to save the memory has been employed (refer to J. Yu et al; J. Mater, Sci. Technol., vol. 23 (2007), p.47-54).
Heat flux due to air gap formation at ingot-mold boundary (refer to Non-Patent Reference 2): the same equation has been applied presented in Table 2 (cooling zone) where
ε ₁ : 0.4 Emissivity on the surface of solid
ε ₂ : 0.35 Emissivity on the inner surface of mold
Heat flux at ingot -chill boundary: Same as those presented in Table 2.

TABLE 6

Casting parameters of IN718 small-sized blade by New DS method (MV2-method)
Dimensions: 6 mm thickness × 42 mm width × 120 mm height
Element partition: Blade part is equally partitioned, 1 mm in X dir., 1.5 mm in Z dir., 1.5 mm in Y dir.
Mold thickness (ceramic mold): 5 mm
Baffle thickness: 10 mm
Heater diameter: 140 mm
Moving speed of brush (moving speed of solidification interface): 40 cm/h
Casting temperature: 1653 K (superheat 46 K)
Initial temperature of mold: 1653 K
Initial temperature of chill: assumed to be 1423 (solidus temperature)-293 = 1130 K. This is a measure to accelerate the timing of reaching steady state.
Radiation heat transfer in the heating region: Approximated by the following equation (see Heat transfer engineering data, 5th edition, Japan Society of Mechanical Engineers (2009), Eq. (41) on p. 139)
$q = \frac{(\sigma A_1(T_1^4 - T_2^4))}{\frac{1}{\epsilon_1} + \frac{A_1}{A_2} \left(\frac{1}{\epsilon_2} - 1 \right)} \quad (W)$
(The above equation is originally applied to radiation heat transfer between coaxial cylindrical surfaces. Here, it is used as an approximate equation.)
σ is Stefan-Boltzmann constant, A ₁ is surface area of heater, A ₂ is surface area of mold, T ₁ is temperature of heater 1500 C., T ₂ is surface temperature of mold, ε ₁ is emissivity of heater 0.35, and ε ₂ is emissivity of mold 0.3
Heat flux of gas cooling at the surface of mold by GCC method (see Non-Patent Reference 2): q = H _{GCC} (Tm - To) (W/m ²)
Heat transfer coefficient by inert gas: H _{GCC} = 600 W/m ² /K
Tm: Surface temperature of mold
To: Atmospheric temperature in cooling zone 500 K
Heat flux due to air gap formation at ingot-mold boundary (see Non-Patent Reference 2): Same as those shown in Table 2
Heat flux at ingot -chill boundary: q = h (T _{g1} - Tc ₂) (W/m ²)
Same as those shown in Table 2 except for h
h: Heat transfer coefficient 168 W/(m ² · K)
Water cooling at the bottom of chill: q = h (T - T _w) (W/m ²)
h: Heat transfer coefficient 168 W/(m ² · K) (Assumed)
T: Chill temperature at the bottom
T _w : Water temperature 293 K

Computational Results

[0100] The computational results are summarized in Table 7(a) and Table 7(b).

TABLE 7(a)

Computational results of IN718 small-sized blades (standard deviations wt %)								
No.	Process	Cr, 19.0	Mo, 3.05	Al, 0.55	Ti, 0.9	Fe, 19.4	Nb, 4.85	Thermal fluctuation in front of solidification interface, K
II-1	Std Bridgman R = 15 cm/h Bz = 0	2.709e-01	4.583e-02	1.043e-02	2.806e-02	2.688e-01	1.537e-01	TI - 17.92 to TI + 22.61 at t = 1190s
II-2	R = Std Bridgman 15 cm/h Bz = 0.5T	1.420e-01	1.598e-02	6.716e-03	2.399e-02	1.273e-01	1.327e-01	No fluctuation
II-3	Std Bridgman 15 cm/h Bz = 0.75T	1.082e-01	1.017e-02	5.455e-03	1.984e-02	9.431e-02	1.110e-01	No fluctuation
II-4	Std Bridgman 15 cm/h Bz = 1T	1.192e-01	1.142e-02	6.024e-03	2.186e-02	1.040e-01	1.222e-01	No fluctuation
II-5	Std Bridgman 15 cm/h Bz = 2T	1.427e-01	1.408e-02	7.230e-03	2.621e-02	1.246e-01	1.463e-01	No fluctuation
II-6	Std Bridgman 15 cm/h Bz = 3T	1.512e-01	1.481e-02	7.656e-03	2.776e-02	1.320e-01	1.550e-01	No fluctuation
II-7	Std Bridgman 15 cm/h Bz = 5T	1.481e-01	1.383e-02	7.463e-03	2.715e-02	1.292e-01	1.519e-01	No fluctuation
II-8	S + sliding brush + GCC 40 cm/h Bz = 0	1.215e-01	2.219e-02	5.449e-03	1.573e-02	1.190e-01	8.584e-02	TI - 26.74 to TI + 20.96 at t = 502s
II-9	S + sliding brush + GCC 40 cm/h Bz = 0.5T	2.813e-02	2.386e-03	1.425e-03	5.225e-03	2.422e-02	2.941e-02	No fluctuation
II-10	S + sliding brush + GCC 40 cm/h Bz = 0.75T	1.990e-02	1.762e-03	1.011e-03	3.639e-03	1.722e-02	2.043e-02	No fluctuation
II-11	S + sliding brush + GCC 40 cm/h Bz = 1T	2.037e-02	1.826e-03	1.039e-03	3.723e-03	1.764e-02	2.090e-02	No fluctuation
II-12	S + sliding brush + GCC 40 cm/h Bz = 2T	2.302e-02	2.169e-03	1.176e-03	4.186e-03	2.005e-02	2.356e-02	No fluctuation
II-13	S + sliding brush + GCC 40 cm/h Bz = 3T	2.596e-02	2.353e-03	1.324e-03	4.720e-03	2.257e-02	2.665e-02	No fluctuation
II-14	S + sliding brush + GCC 40 cm/h Bz = 5T	2.986e-02	2.449e-03	1.507e-03	5.442e-03	2.584e-02	3.081e-02	No fluctuation

Note 1:

No. II-1 to No. II-7 are by simple M-method, dt = 2s. No. II-8 to No. II-14 are by MV2-method, dt = 1s. S denotes single chamber.

Note 2:

Thermal fluctuation is defined by $TI \pm dT$, where TI (1607 K) is liquidus temperature.

TABLE 7(b)

Computational results of IN718 small-sized blades (Min, Max and average value of standard deviation wt %)							
No	Process	Cr, 19.0 Min-Max (Ave)	Mo, 3.05 Min-Max (Ave)	Al, 0.55 Min-Max (Ave)	Ti, 0.9 Min-Max (Ave)	Fe, 19.4 Min-Max (Ave)	Nb, 4.85 Min-Max (Ave)
II-1	Std Bridgman R = 15 cm/h Bz = 0	17.494-19.547 (19.016)	2.781-3.107 (2.996)	0.495-0.575 (0.534)	0.773-1.002 (0.854)	17.905-19.881 (19.388)	4.157-5.379 (4.597)
II-8	S + sliding brush + GCC 40 cm/h Bz = 0	18.305-19.453 (19.110)	2.870-3.051 (3.028)	0.511-0.550 (0.541)	0.811-0.901 (0.871)	18.658-19.800 (19.489)	4.366-4.857 (4.687)
II-10	S + sliding brush + GCC 40 cm/h Bz = 0.75T	18.984-19.111 (19.068)	3.042-3.052 (3.046)	0.544-0.551 (0.547)	0.880-0.901 (0.888)	19.381-19.497 (19.458)	4.735-4.854 (4.779)

In Table 7, 'S' means Single chamber apparatus of MV2-method. While the single chamber, sliding brush, GCC and the magnet for exerting axial magnetic field Bz are the basic components of MV2-method, the speed of the sliding brush, Bz and the cooling intensity by GCC are the operating parameters to be defined case by case.

FIG. 11 shows the effect of Bz on the normalized standard deviation for each alloying elements by the MV2 method (σ are normalized by C0 to make it easier to see the relative values among elements). For each alloy elements, σ/C_0 reach a minimum around Bz=0.75T, after which σ/C_0 increase inversely with increasing Bz. The effect of Bz on the standard deviation σ (wt %) of Nb by the M method and MV2 method is shown in FIG. 12. FIGS. 13 and 14 respectively show the distributions of DAS and Nb in the axial direction at the cross sectional center, using the M method. Since DAS depends primarily on the solidification rate, it does not change with Bz (FIG. 13). On the other hand, in the case of the Nb distribution without magnetic field, the liquid flow pattern within the mushy zone is disturbed by thermal fluctuation, resulting in a large variation of about 0.3 wt % ($0.3/C_0 \times 100 = 6.2\%$) as shown in FIG. 14. In contrast, when magnetic field is applied, the thermal fluctuation disappears and the flow pattern stabilizes, resulting in much

smaller variations, but the standard deviation itself is not so small as shown in FIG. 12. This is because the liquid flow pattern within the mushy zone changed due to the application of the magnetic field (flow from the center to the periphery, not shown for simplicity), resulting in a rather large change in Nb for the entire blade.

[0101] FIGS. 11 and 12 show that when the withdrawal speed is increased from 15 cm/h to 40 cm/h (i.e., moving speed of sliding brush) and the cooling intensity is increased ($H_{gcc} = 600 \text{ W/m}^2/\text{K}$), the standard deviation becomes much smaller (change from No. II-1 to No. II-8). Thus, macrosegregation is greatly improved. Furthermore, when an axial static magnetic field Bz is applied to No. II-8, σ (and σ/C_0) decreases further and reaches a minimum around Bz=0.75T. Thereafter, σ gradually increases as Bz is increased.

[0102] When the moving velocity of the solidification interface is increased from 15 cm/h to 40 cm/h (in comparison between No. II-1 and No. II-8), σ decreases because the

turbulent flow in the mushy zone is reduced. However, thermal fluctuations in front of the solidification interface are still on the order of $\pm 20^\circ$ C. (No. II-1) and $\pm 23^\circ$ C. (No. II-8), respectively, creating significant convection (velocity in the bulk liquid zone is also on the order of $V_{\max}=1.08$ cm/s and 0.88 cm/s, respectively, at the time $\frac{1}{2}$ solidified and in (Y, Z) cross section at the center of thickness direction). On the other hand, when B_z is applied, the flow pattern in the bulk liquid zone tends to change from turbulent to laminar, with downward laminar flow at the minimum value of $B_z=0.75$ T, and the flow pattern within the mushy zone becomes also almost laminar. Then, thermal fluctuations in front of the interface disappear (not shown for want of space).

[0103] [Note: The values of the velocity vectors are herein expressed in terms of the (X, Y) plane as $v=\sqrt{v_x^2+v_y^2}$, (Y, Z) plane as $v=\sqrt{v_y^2+v_z^2}$, and (X, Z) plane as $v=\sqrt{v_x^2+v_z^2}$. The same is true for Lorentz forces]

[0104] As the intensity is increased from $B_z=0.75$ T, σ gradually increases. This is due to an increase in the driving force (i.e., thermoelectromagnetic force, TEMF) that makes the liquid phase flow due to the interaction between the thermoelectromotive force caused by the temperature gradient and the magnetic field, as described below (see paragraph 0073).

[0105] FIG. 15 shows the comparison of DAS distributions for each process (in Z-direction at the XY cross-sectional center).

While $DAS=180$ μm for No. II-1 (Standard Bridgman, 15 cm/h, $B_z=0$), DAS were refined to $115\sim 120$ μm for No. II-8 (MV2: S+sliding brush+GCC, 40 cm/h, $B_z=0$), No. II-10 (MV2: S+sliding brush+GCC, 40 cm/h, $B_z=0.75$ T), and No. II-13 (MV2: S+sliding brush+GCC, 40 cm/h, $B_z=3$ T). Also, the variation ranges were reduced from 20 μm to the order of 5 μm .

[0106] FIG. 16 shows the comparison of the Nb distributions at the same locations as FIG. 15. Compared with No. II-1 and No. II-8 without magnetic fields, the segregation variations in No. II-10 and No. II-13 with B_z applied improved to a large extent and at the same time approached the initial content of 4.85 wt %, indicating that the homogeneities were improved.

Discussion: On the Flow Pattern of Liquid Phase

[0107] As described in Paragraph 0065, when no magnetic field is applied, thermal fluctuations in front of the solidification interface are on the order of $\pm 20^\circ$ C. (No. II-1) and $\pm 23^\circ$ C. (No. II-8), respectively, which causes significant convection, disturbs the shape of the solidification interface, and disturbs the flow pattern within the mushy zone. In contrast, in No. II-10, where $R=40$ cm/h and the optimum magnetic field ($B_z=0.75$ T) was applied, the flow in the bulk liquid zone was almost rectified in the axial direction, and the maximum flow velocities on the order of $V_{\max}=1.08$ cm/s (No. II-1) and 0.88 cm/s (No. II-8) were suppressed to $V_{\max}=0.04$ cm/s (No. II-10). The thermal fluctuations in front of the interface disappeared, and the shape of the interface became stable; the flow within the mushy zone was nearly rectified in the axial direction (slightly fan-shaped at both ends in the width direction).

[0108] When B_z is applied, Lorentz force ($f=J\times B$) acting on the liquid phase occurs in the horizontal directions, not in the axial direction. The Lorentz force and flow patterns in

the mushy zone are outlined in FIGS. 17(a) and 17(b), respectively, for No. II-10. In response to the f pattern, one vortex and two semi-vortexes were formed in (X, Y) plane. When B_z is increased in the range of $B_z=0$ to 0.75 T, the turbulent flow within the mushy zone settles down to the flow pattern as shown in Figure (b) in response to the Lorentz force pattern shown in Figure (a), i.e., the turbulence of the flow disappears. The horizontal velocity components (V_x and V_y) are extremely small compared with V_z , the velocity component in the Z direction, and are much slower than the moving velocity of the solidification interface ($R=40$ cm/h= 0.011 cm/s), and therefore have little effect on macrosegregation. The above is the mechanism for suppressing convection by the static magnetic field, which accordingly reduced the σ of Nb from 0.1537 wt % (No. II-1) to 0.0204 wt % (No. II-10) (see Table 7). The above magnetic fields are referred to as low magnetic fields herein.

[0109] As the magnetic field strength is increased from $B_z=0.75$ T, the Lorentz force in the horizontal directions in the XY plane gradually increases. At $B_z=5$ T, the Lorentz force in the aforementioned mushy zone (XY plane at the location shown in FIG. 17) increases from $f_{\max}=5.82$ dyn/cm³ ($B_z=0.75$ T) to $f_{\max}=41.4$ dyn/cm³ and the flow velocity $V_{\max}=3.6\times 10^{-5}$ cm/s ($B_z=0.75$ T) to $V_{\max}=2.2\times 10^{-4}$ cm/s. The flow pattern is basically unchanged. The flow pattern in the bulk liquid zone also remains basically the same, and the maximum flow velocity V_{\max} (No. II-10, time 502 sec, YZ section at the center of the wall thickness) decreases from 0.043 cm/s ($B_z=0.75$ T) to 0.01 cm/s. In other words, the gradual increase in σ from the minimum value ($B_z=0.75$ T) is due to the gradual increase of the detrimental horizontal velocity components within the mushy zone (see FIG. 12). In this description, such a field range is referred to as the medium field.

[0110] The flow pattern within the mushy zone is determined by the balance between the thermoelectromagnetic force (TEMF) as a driving force, the electromagnetic braking force (EMBF), and the force generated by the electric field strength and B_z ($\sigma\nabla\phi\times B$). In this case, the TEMF is dominant in the range from a low magnetic field of $B_z=0.75$ T to a relatively high magnetic field of $B_z=5$ T (i.e., low to medium fields). In this example, the minimum value of σ is around $B_z=0.75$ T, so it makes no practical sense to make it stronger than this, and so further discussion is omitted.

Discussion: On Solidified Microstructure

[0111] The refinement and homogeneity of the microstructure improves creep strength, and shortens the time required for solution annealing (i.e. heat treatment for solutionizing microsegregation of the dendrite arm spacing range or the second phases such as γ' phase (gamma prime) and carbides into the γ matrix) and subsequent aging time (i.e. heat treatment to precipitate γ' phase from γ matrix) after the casting of Ni-base alloys. For example, the time required for solution annealing is roughly proportional to DAS^2/D_s (D_s are the diffusion coefficients of the alloying elements in the solid phase), so that, if DAS is reduced to $\frac{1}{2}$, the time required is reduced to $\frac{1}{4}$ (see p. 332, Eq. (10-6) of Non-Patent Reference 7).

Principles of the Present Invention

[0112] Liquid flow within the mushy zone is caused by solidification contraction due to the density difference

between the liquid and solid phases (the treatment of flow in the mushy zone is described in Paragraph 0042, C. Method of Solidification Analysis, but here we focus on the solidification contraction). In other words, the driving force for the flow is the suction force associated with solidification contraction, which is transmitted sequentially from the root of the dendrite to the tip of the dendrite. Therefore, (1) the higher the cooling intensity of the solid phase region and the faster the moving speed R of the mushy zone, the stronger this tendency becomes, and as a result, the flow pattern is considered to become stronger in the axial direction. In the simulations of Specific Examples 1 and 2, the reason why the segregation standard deviation σ decrease with increasing cooling intensity and increasing R is because the flow pattern tend to align in the axial direction, which theoretically and quantitatively proves the validity of the above mechanism.

[0113] However, as mentioned above, even if the cooling is intensified and R is increased, the heat pulses in front of the solidification interface cannot be eliminated, and the flow pattern within the mushy zone remains disturbed. Then, this inventor has shown that (2) by applying an axial static magnetic field onto the whole mushy zone, the heat pulses at the solidification interface can be eliminated and σ can be reduced. Thus, the flow within the mushy zone can be rectified in the axial direction.

[0114] The synergistic effect of above (1)+(2) effectively rectifies the flow within the mushy zone in the axial direction and stabilizes solidification, thereby eliminating macrosegregation and suppressing misoriented grain defects. [Note: The above principles are applicable regardless of whether the process is upward or downward or a mixture of the two types of buoyancy.]

Other Characteristics

[0115] (1) Static Solid Cooling (SSC)

[0116] Recently, Lian et al. (Non-Patent Reference 14) proposed a method to enhance cooling capability by using Pyrolytic Graphite (PG, pyrolytic graphite) molds with high thermal conductivity and high thermal diffusivity. A schematic diagram is shown in FIG. 18. In this method, the mold is surrounded by a laminated solid consisting of alternating heat transfer layer (PG layer) and insulation layer, inside of which another laminated solid is placed so as to follow up the shape of the blade. The mold itself is coated with a very thin coating. Heating and cooling are done by resistance heaters and water cooling, respectively, located around the periphery of the heat transfer layer. Directional solidification is performed by moving the heating-cooling cycle step by step upward through an electrical network. They state that this method provides much higher cooling capability than GCC or LMC.

[0117] It is also possible to use the SSC mold as an intensified cooling method in the present invention. However, the heating and cooling means are based on the inventive means of the present application (FIG. 19 shows an example of using the mold by the SSC method in the MV2 method of the present application).

[0118] (2) The purpose of the sub-heater in the heating means is to prevent the temperature drop of the solidification interface temperature of the mushy zone and thereby prevent the drop of the axial temperature gradient of the mushy zone.

[0119] In this description, a parallel static magnetic field B_z is applied to the entire mushy zone and the bulk liquid zone for the sake of simulations, but this is not necessarily required for actual operation. It may apply at least onto the whole mushy zone (in this case, the parallel magnetic field effectively covers a fairly wide area above the solidification interface).

[0120] (3) Although there is no clear definition for the cooling intensity in directional solidification, the Non-Patent Reference 2, for example, assumes a simple heat transfer model and roughly estimates the heat flux Q for large blades as follows: $Q=60 \text{ kW/m}^2$ (weak cooling) for the Bridgman method; $Q=86 \text{ kW/m}^2$ for the LMC method using molten tin; and $Q=101 \text{ kW/m}^2$ for the GCC method. In this description, cooling by LMC, GCC, and the SSC method mentioned above is referred to as strong cooling.

[0121] There is no clear definition for the strength of the static magnetic field as well, but in this description, the magnetic fields as used in Paragraphs 0035, 0061, 0072, and 0074 (all 1 T or less) are referred to as low magnetic fields; the magnetic fields described in Paragraph 0073 (1 to about 3 T) are referred to as medium magnetic fields. However, there is no clear definition for the boundaries between these fields.

[0122] (4) Other factors that affect solidification include the size and shape (i.e. expansion/contraction of the cross section) of the castings and the thickness of the insulation baffles. The shape of the mushy zone is determined by these casting conditions, which is desirable as flat as possible. For these matters, CPRO simulation should be performed to adjust the speed of moving solidification interface, heating and cooling conditions, etc. (refer to Solidification Monitoring System described later).

[0123] (5) Although banding type segregation has been described herein, macrosegregation can take various forms depending on alloy composition, blade size and shape, casting parameters, etc., and is ultimately determined by the flow pattern within the mushy zone. Regardless of the form, these defects can be eliminated by suppressing convection in the bulk liquid zone, eliminating heat pulses, and substantially rectifying the flow pattern within the mushy zone. Thus, the findings obtained herein have generality and universality for macrosegregation problems encountered in directional solidification. The similar effect is observed for mis-oriented grain defects as well.

SUMMARY

[0124] The features and advantages of the MV1 and MV2 methods are summarized as follows. (They are described with respect to the directional solidification of Ni-based alloy SX or DS turbine blades.)

[0125] (1) Elimination of macrosegregation and mis-oriented grain defects: Convection in the bulk liquid zone is quenched and heat pulses at the solidification interface are eliminated by strongly cooling the solid phase region, increasing the moving velocity of the solidification interface, and applying an axial static magnetic field (B_z) onto the whole mushy zone. These synergistic effects suppress detrimental lateral liquid flow in the mushy zone and rectify it in the axial direction. These

effects eliminate macrosegregation and stabilize solidification, thereby eliminating the causes of misoriented grain defects.

[0126] It was, then, found that there is a region where the macrosegregation standard deviation becomes minimized when the magnetic field is increased in a relatively low magnetic field range, and that although the effect is still present, further increase results in rather a wasteful energy level. This effect was discovered for the first time by the present invention, which has made it possible to keep the required magnetic field strength at relatively low. [As mentioned in Paragraph 0021, when the liquid flow within the mushy zone is rectified in the axial direction, macrosegregation does not occur (refer to Non-Patent Reference 7, p. 252, FIGS. 7-35)]

[0127] (2) Refinement and homogenization of microstructure: The synergistic effect of the above-mentioned axial static magnetic field (Bz) and the strong cooling of the solid phase region can refine and homogenize the microstructure, thus greatly reducing the solution heat treatment time after casting (improvement of productivity).

[0128] (3) Improved economy and productivity: Compared with the simple M method, this method provides its effectiveness with a much smaller axial static magnetic field (Bz), which makes it possible to greatly reduce the price of expensive superconducting coils. Also, productivity can be increased by increasing the withdrawal speed.

[0129] The above features and advantages are significant improvements over the conventional simple M method (i.e., Standard Bridgman method+Bz described in the applicant's Patent Reference 3 and Non-Patent Reference 6), and are the findings revealed for the first time in this description.

[0130] As described above, high-quality turbine blades with excellent creep rupture strength and no macrosegregation or misoriented grain defects can be efficiently produced. Also, it should be noted that a desired microstructure (DAS) can be obtained by adjusting the cooling intensity in the solid phase region and Bz. Although the GCC method was used as the strong cooling means in this example, it is clear in principle that the same effect can be obtained by the LMC method having almost the same cooling capability, or by using a mold made of Static Solid Cooling method, which has even higher cooling capability.

Real-Time Solidification Monitoring System

[0131] The present invention is equipped with a real-time solidification monitoring system for monitoring the solidification status when performing directional solidification based on predetermined casting parameters (operating parameters). This enables to efficiently establish optimal casting conditions for manufacturing high-quality blades for each product in a short period of time. FIG. 20 shows an overview of the solidification monitoring system incorporating the solidification simulation system CPRO.

[0132] In FIG. 20, 61 is the detection section, which detects each of the operation parameters described below and outputs them as data. Also, 62 is a computer, which processes the data output from the detection section 61 as input conditions to perform a solidification simulation using CPRO, as described in detail in the Specific Examples 1 and 2. The computer has the function of processing the solidification state so that it can be imaged and observed.

[0133] 63 and 64 are monitoring devices connected to said computer 62. The monitoring device 63 is used to display the operating parameters, and the monitoring device 64 is used to display the images of solidification simulation results.

[0134] The measurement items of the operational parameters in the detection section 61 of FIG. 20 are as follows. In the case of the MV1 method:

[0135] Powers and temperatures for the main and sub heaters

[0136] Temperatures of the mold and casting

[0137] Heat transfer coefficient at the mold surface by GCC or temperature of molten metal bath by LMC

[0138] Water volume, water temperature, and chill surface temperature of water-cooled chill jacket

[0139] Withdrawal speed of the mold

[0140] Voltage, current, and static magnetic field strength of superconducting magnet or conventional electromagnetic magnet

[0141] Degree of vacuum in the vacuum chamber

[0142] For MV2 method:

[0143] Powers and temperatures for the main and sub heaters

[0144] Temperatures of the mold and casting

[0145] Heat transfer coefficient and temperature at the mold surface by GCC

[0146] Water volume, water temperature, and chill surface temperature of the water-cooled chill jacket

[0147] Moving speed of sliding brush system

[0148] Voltage, current, and static magnetic field strength of superconducting magnet or conventional electromagnetic magnet

[0149] Degree of vacuum in the vacuum chamber

[0150] The real-time monitoring items are as follows.

[0151] Temperatures of the casting and mold

[0152] Temperature gradient at the solidification interface and the shape of mushy zone

[0153] DAS distribution

[0154] Monitoring the presence of macrosegregation by displaying the superposition image of liquid phase velocity+segregation+volume fraction solid

[0155] Monitoring the presence of misoriented grain defects by displaying the macrostructure

On the Operation of Solidification Monitoring System

[0156] The monitoring system thus enables visualization of the solidification phenomena such as temperature change and distribution, the shape of mushy zone, liquid phase flows in the bulk liquid zone and mushy zone, and the formation of macrosegregation, etc. that change from moment to moment, so that it makes it possible to observe in real time the solidification phenomena that were previously unknown as a black box. This enables a deeper understanding of solidification phenomena.

[0157] Therefore, the number of casting experiments based on the conventional trial-and-error or a statistical method of Design-of-experiments can be minimized or eliminated, and the excessive time and cost for such experiments can be significantly reduced.

[0158] The main points of the above operational method are as follows:

[0159] (1) The simulation is highly accurate because it is based on actual measurement data.

[0160] (2) The system is installed both at the production site (on-site computer) and at a remote location (off-site

computer), so that at the production site, one can monitor real-time and at a remote location such as laboratory one can use for research and development.

[0161] (3) Optimal casting conditions (operating parameters mentioned above) are determined for each product.

INDUSTRIAL APPLICABILITY

[0162] Although the present invention has been described for Ni—Al alloy and Ni-based superalloy IN718, it is clear in principle that this invention can be applicable for such alloy systems as Ni-based Superalloys, Titanium alloys, Co-based alloys, Fe-based alloys, and so on that exhibit dendrites or cellular structures in the solidification process. Therefore, these alloy systems are subject to the present invention.

[0163] As described above, this invention enables the production of high-quality directionally solidified castings or ingots such as Ni-based superalloy turbine blades, and will greatly contribute to energy conservation and global warming countermeasures by increasing the safety and longevity of these important components and improving efficiency of gas turbine. It is widely known that the most effective way to increase the combustion efficiency of gas turbines for power generation is to raise the combustion gas inlet temperature of the turbine, and this invention can raise the inlet temperature by enabling the practical use of large single crystal blades that can withstand harsh operating environments (Effects of the single crystallization of the blade material include an increase in the melting point and creep strength).

[0164] On the other hand, in the field of jet engines for aircraft, single-crystal Ni-based superalloy turbine blades are already in practical use. However the application of this invention will further improve the casting yield and contribute to fuel efficiency and CO₂ reduction.

Explanation of Reference Symbols

[0165]	1	Mold
[0166]	2	Casting or Ingot (molten metal)
[0167]	3	Selector
[0168]	4	Cooling chill (water-cooled chill)
[0169]	5a	Main heater
[0170]	5b	Sub-heater
[0171]	6	Insulating sleeve
[0172]	7	Insulating top cover
[0173]	8	Pouring spout
[0174]	9	Insulation baffle
[0175]	10	Induction melting furnace
[0176]	11	Cooling gas nozzle
[0177]	12	Cooling gas outlet
[0178]	13	Cooling gas circulation pump system
[0179]	14	Superconducting coil
[0180]	15	Vacuum pump
[0181]	16	Vacuum vessel
[0182]	17	Outer casing
[0183]	18	Molten metal bath
[0184]	19	Stainless steel chill
[0185]	20	Molten metal bath container
[0186]	21	Mold withdrawing arm (stainless steel)
[0187]	22	Insulation layer (alumina beads)
[0188]	23	Stirrer

[0189]	24	Induction melting furnace with under pouring spout
[0190]	25	MV2 method: Main heater
[0191]	26	MV2 method: Insulating sleeve
[0192]	27	MV2 method: Main heater sliding contact terminal
[0193]	28	MV2 method: Main heater sliding brush
[0194]	29	MV2 method: Main heater power supply
[0195]	30	MV2 method: Sub-heater
[0196]	31	MV2 method: Copper cable for sub-heater
[0197]	32	MV2 method: Sub-heater power supply
[0198]	33	MV2 method: Insulation baffle
[0199]	34	MV2 method: Cooling gas inlet pipe
[0200]	35	MV2 method: Cooling gas nozzle
[0201]	36	MV2 method: Cooling gas suction port
[0202]	37	MV2 method: Cooling gas circulation pump system
[0203]	38	MV2 method: Vacuum pump
[0204]	39	MV2 method: Mold containing outer chamber
[0205]	40	MV2 method: Superconducting coil
[0206]	61	Detection section of directional solidification
[0207]	62	System computer (on-site/off-site)
[0208]	63	Monitor for displaying operating parameters
[0209]	64	Monitor for displaying images of solidification simulation results

1. A directional solidification apparatus for making directionally solidified castings or ingots having a grain structure consisting of a single crystal structure, or a polycrystalline columnar dendrite structure or a mixture of said single crystal structure and said polycrystalline columnar dendrite structure, wherein

- (1) a first means of said directional solidification apparatus includes a mold for casting molten metal, an adiabatic baffle for dividing said mold into a heating region to heat said mold and a cooling region to cool said mold during directional solidification process, a means for moving said mold from said heating region to said cooling region, a heating means for heating and keeping said molten metal in said mold at a prescribed temperature, and a fierce cooling means for enhancing the heat removal capability from a side surface of said mold so as to rectify the liquid flow within a solid-liquid coexisting phase in a directional solidification direction, and by moving said mold at a prescribed speed to accomplish said directional solidification process, and
- (2) during said directional solidification process, a second means is provided which applies a static magnetic field onto at least the entire solid-liquid coexisting phase in a direction substantially parallel to the directional solidification direction to suppress convection in the liquid phase, thereby eliminates heat pulses at the solidification interface and suppresses turbulent liquid flow within said solid-liquid coexisting phase so as to rectify in the directional solidification direction, and, said directional solidification apparatus is characterized by synergistic effects based on the respective rectifying effects of said first means of (1) and said second means of (2) so that said synergistic effects suppress the formation of macrosegregation or mis-oriented grain defects and refine the microstructure.

2. The directional solidification apparatus described in claim 1, wherein said heating means is equipped with a main

heater by resistance heating and at least one resistance sub-heater located directly above said insulating baffle.

3. The directional solidification apparatus described in claim 1, wherein said fierce cooling means is configured to cool said mold in that a nozzle for an inert gas is placed immediately under the insulating baffle to blow said inert gas against the side surface of said mold.

4. The directional solidification apparatus described in claim 1, wherein said fierce cooling means is configured to cool said mold by immersing said mold in a molten metal bath made of a low-melting-point material.

5. The directional solidification apparatus described in claim 1, wherein said mold is formed by alternating layers of graphite having high thermal conductivity and thermally insulating material.

6. A directional solidification method for making directionally solidified castings or ingots having a grain structure consisting of a single crystal structure, or a polycrystalline columnar dendrite structure or a mixture of said single crystal structure and said polycrystalline columnar dendrite structure, wherein

(1) a first step of a directional solidification process, wherein molten metal is cast into a mold and cooled to produce said directionally solidified castings or ingots, consists of

a heating region to heat said mold,
 a cooling region to cool said mold, and
 a thermally insulating region between said heating region and said cooling region, and
 moving said mold from said heating region to said cooling region to proceed directional solidification, wherein in said heating region the molten metal in said mold is heated and kept at a prescribed temperature, and in said cooling region the solid region is strongly cooled so as to rectify the liquid flow within the solid-liquid coexisting phase in directional solidification direction and said mold is moved at a prescribed speed to accomplish said directional solidification, and

(2) during said directional solidification process, a second step is provided which applies a static magnetic field in a direction substantially parallel to said directional solidification direction onto at least the entire solid-liquid coexisting phase in order to suppress convection in the liquid region, thereby eliminates heat pulses at the solidification interface and suppresses turbulent liquid flow within said solid-liquid coexisting phase, and,

said directional solidification method is characterized by synergistic effects based on the respective rectifying effects of said first step of (1) and said second step of (2) so as to suppress the formation of macrosegregation or misoriented grain defects and refine the microstructure.

7. The directional solidification method described in claim 6, wherein a method to heat said mold is characterized by heating around the lower edge of said heating region and directly above said insulating region so as to heat and keep said molten metal in said mold at a prescribed temperature.

8. The directional solidification method described in claim 6, wherein a method to cool said mold is characterized by blowing an inert gas onto the side surface of said mold.

9. The directional solidification method described in claim 6, wherein a method to cool said mold is characterized by immersing said mold in a molten metal bath made of a low-melting-point material.

10. The directional solidification method described in claim 6, wherein said mold is formed by alternating layers of graphite having high thermal conductivity and thermally insulating materials.

11. In a directional solidification apparatus for producing castings or ingots having a grain structure consisting of a single crystal structure or a polycrystalline columnar dendrite structure or a mixed structure of said single crystal structure and said polycrystalline columnar dendrite structure, wherein a heating region for heating a mold, a strong cooling region for cooling the mold, and an insulating region for thermally separating and blocking these two regions are contained in a single chamber which is equipped with:

said mold for casting the castings or ingots,
 a cooling chill at the bottom of said mold to initiate solidification,

a sliding heat resistant main heater for heating said mold, an insulating sleeve to support said main heater and block heat radiation to the outside,

a mold cooling gas nozzle to cool said mold, and an insulating baffle located on the upper part of said mold cooling gas nozzle,

said insulating baffle and said mold cooling gas nozzle being able to move up and down synchronously and integrally,

said main heater providing with a passage to allow said insulating baffle and said mold cooling gas nozzle to move up and down together,

said main heater connecting to sliding contact terminals set up on the outside of said insulation sleeve, and said sliding contact terminals contacting with a sliding brush,

power supplied range between the upper end of said main heater and said sliding brush being variable by sliding said sliding brush up and down synchronously and integrally with said insulating baffle and said mold cooling gas nozzle,

said single chamber is also provided with means for applying a static magnetic field in a direction substantially parallel to said directional solidification direction onto an entire solid-liquid coexisting phase in said mold,

and at the start of operation, said sliding brush, said insulating baffle and said mold cooling gas nozzle are positioned at the lower end of said mold,

power is supplied to the energized region to heat and keep said mold at a prescribed temperature above the melting point of the metal material after melting and casting of said metal material,

the performance of directional solidification of said casting or ingot is characterized by supplying cooling gas to said mold cooling gas nozzle while reducing said heating region by moving said energized region upward at a prescribed speed and at the same time applying said static magnetic field onto said entire solid-liquid coexisting phase in a direction substantially parallel to the directional solidification direction.

12. The directional solidification apparatus described in claim 11, wherein a heating means is equipped with at least

one resistance sub-heater located directly above said insulating baffle to heat around the lower edge of said heating region

13. The directional solidification apparatus described in claim **11**, wherein said mold is formed by alternating layers of graphite having high thermal conductivity and thermally insulating materials.

14. A directional solidification method for producing castings or ingots having a grain structure consisting of a single crystal structure or a polycrystalline columnar dendrite structure or a mixed structure of said single crystal structure and said polycrystalline columnar dendrite structure, wherein a heating region for heating a mold, a strong cooling region for cooling the mold, and an insulating region for thermally separating and blocking these two regions are contained in a single chamber,

wherein a heating method for heating said mold is done by resistance heating the energized range between a fixed position at an upper end of said heating region and a lower end of said heating region whose said energized range reduces and varies and at the same time said mold is strongly cooled by blowing inert gas against a side surface of said mold,

and at the start of operation, said energized region surrounds said entire mold to heat and keep said mold at a prescribed temperature above the melting point of the metal material, and after melting and casting said metal material, said energized range is reduced at a prescribed speed from the lower end of said mold to a position fixed at said upper end, while strongly cooling the lower region under said insulating region to solidify and at the same time a static magnetic field is exerted onto at least an entire solid-liquid coexisting phase of said casting or ingot in a direction substantially parallel to the directional solidification direction.

15. The directional solidification method described in claim **14**, wherein said heating method is equipped with at least one resistance sub-heater located directly above said insulating region to heat around the lower end of said heating region.

16. The directional solidification method described in claim **14**, wherein said mold is formed by alternating layers of graphite having high thermal conductivity and thermally insulating materials.

17-22. (canceled)

* * * * *